

# The TRAPP complex mediates secretion arrest induced by stress granule assembly

Francesca Zappa<sup>1,\*</sup> , Cathal Wilson<sup>1</sup>, Giuseppe Di Tullio<sup>1</sup>, Michele Santoro<sup>1</sup>, Piero Pucci<sup>2</sup>, Maria Monti<sup>2</sup>, Davide D'Amico<sup>1</sup>, Sandra Pisonero-Vaquero<sup>1</sup>, Rossella De Cegli<sup>1</sup>, Alessia Romano<sup>1</sup>, Moin A Saleem<sup>3</sup>, Elena Polishchuk<sup>1</sup>, Mario Failli<sup>1</sup>, Laura Giaquinto<sup>1</sup> & Maria Antonietta De Matteis<sup>1,2,\*\*</sup> 

## Abstract

The TRANsport Protein Particle (TRAPP) complex controls multiple membrane trafficking steps and is strategically positioned to mediate cell adaptation to diverse environmental conditions, including acute stress. We have identified the TRAPP complex as a component of a branch of the integrated stress response that impinges on the early secretory pathway. The TRAPP complex associates with and drives the recruitment of the COPII coat to stress granules (SGs) leading to vesiculation of the Golgi complex and arrest of ER export. The relocation of the TRAPP complex and COPII to SGs only occurs in cycling cells and is CDK1/2-dependent, being driven by the interaction of TRAPP with hnRNPK, a CDK substrate that associates with SGs when phosphorylated. In addition, CDK1/2 inhibition impairs TRAPP complex/COPII relocation to SGs while stabilizing them at ER exit sites. Importantly, the TRAPP complex controls the maturation of SGs. SGs that assemble in TRAPP-depleted cells are smaller and are no longer able to recruit RACK1 and Raptor, two TRAPP-interactive signaling proteins, sensitizing cells to stress-induced apoptosis.

**Keywords** Cdk; COPII; integrated stress response; stress granules; TRAPP complex

**Subject Category** Membranes & Trafficking

**DOI** 10.15252/emj.2019101704 | Received 4 February 2019 | Revised 31 July 2019 | Accepted 1 August 2019

**The EMBO Journal (2019) e101704**

## Introduction

The TRAPP (TRANsport Protein Particle) complex is a conserved multimolecular complex intervening in multiple segments of membrane trafficking along the secretory, the endocytic, and the autophagy pathways (Kim *et al*, 2016).

Originally identified in yeast as a tethering factor acting in ER-to-Golgi trafficking, it was subsequently discovered to act as a GEF for

Ypt1 and Ypt31/32 in yeast and for Rab1 and possibly Rab11 in mammals (Yamasaki *et al*, 2009; Westlake *et al*, 2011; Zou *et al*, 2012). The TRAPP complex has a modular composition and is present as two forms in mammals: TRAPP<sup>II</sup> and TRAPP<sup>III</sup> which share a common heptameric core (TRAPPC1, TRAPPC2, TRAPPC2L, TRAPPC3, TRAPPC4, TRAPPC5, TRAPPC6) and additional subunits specific for TRAPP<sup>II</sup> (TRAPPC9/TRAPPC10) or for TRAPP<sup>III</sup> (TRAPPC8, TRAPPC11, TRAPPC12, TRAPPC13; Sacher *et al*, 2018). TRAPP<sup>II</sup> has been implicated in late Golgi trafficking while TRAPP<sup>III</sup> has a conserved role in the early secretory pathway (ER-to-Golgi) and in autophagy (Yamasaki *et al*, 2009; Scrivens *et al*, 2011). Recent lines of evidence have expanded the range of activities of the TRAPP complex by showing that it takes part in a cell survival response triggered by agents that disrupt the Golgi complex (Ramírez-Peinado *et al*, 2017) and can drive the assembly of lipid droplets in response to lipid load (Li *et al*, 2017).

The importance of the TRAPP complex in humans is testified by the deleterious consequences caused by mutations in genes encoding distinct TRAPP subunits. Mutations in TRAPPC2L, TRAPPC6A, TRAPPC6B, TRAPPC9, and TRAPPC12 cause neurodevelopmental disorders leading to intellectual disability and dysmorphic syndromes (Khattak & Mir, 2014; Milev *et al*, 2017, 2018; Harripaul *et al*, 2018; Mohamoud *et al*, 2018), mutations in TRAPPC11 lead to ataxia (Koehler *et al*, 2017), and mutations in TRAPPC2 lead to the spondyloepiphyseal dysplasia tarda (SED; Gedeon *et al*, 1999).

Spondyloepiphyseal dysplasia tarda is characterized by short stature, platyspondyly, barrel chest, and premature osteoarthritis that manifest in late childhood/prepubertal age. We have shown that pathogenic mutations or deletion of TRAPPC2 alter the ER export of procollagen (both type I and type II) and that TRAPPC2 interacts with the procollagen escort protein TANGO1 and regulates the cycle of the GTPase Sar1 at the ER exit sites (ERES; Venditti *et al*, 2012). The Sar1 cycle in turn drives the cycle of the COPII coat complex, which mediates the formation of carriers containing neo-synthesized cargo to be transported to the Golgi complex. While this role of TRAPPC2 in the ER export of PC might explain the altered ECM deposition observed in patient's cartilage (Tiller *et al*, 2001;

1 Telethon Institute of Genetics and Medicine, Pozzuoli (Naples), Italy

2 Federico II University, Naples, Italy

3 Bristol Renal, Bristol Medical School, University of Bristol, Bristol, UK

\*Corresponding author. Tel: +1 8058 375229; E-mail: Fzappa@ucsb.edu

\*\*Corresponding author. Tel: +39 8119 230620; E-mail: dematteis@tigem.it

Venditti *et al*, 2012), it leaves the late onset of the disease signs unexplained. We hypothesized that the latter could be due to an inability to maintain long-term cartilage tissue homeostasis, possibly due to an impaired capacity of chondrocytes to face the physiological stresses that underlie and guide their development and growth. These include mechanical stress that can induce oxidative stress leading to apoptosis (Henrotin *et al*, 2003; Zuscik *et al*, 2008).

Here, by analyzing the cell response to different stresses, we show that TRAPPC2 and the entire TRAPP complex are components of stress granules (SGs), membrane-less organelles that assemble in response to stress (Protter & Parker, 2016).

The recruitment of TRAPP to SGs has multiple impacts on the stress response as it induces the sequestration of Sec23/Sec24 (the inner layer of the COPII complex) onto SGs thus inhibiting trafficking along the early secretory pathway, leads to the inactivation of the small GTPase Rab1 with a consequent disorganization of the Golgi complex, and is required for the recruitment of signaling proteins, such as Raptor and RACK1, to SGs thus contributing to the anti-apoptotic role of SGs. Interestingly, TRAPP and COPII recruitment to SGs only occurs in actively proliferating cells and is under control of cyclin-dependent kinases (CDK 1 and 2).

The TRAPP complex thus emerges as a key element in conferring an unanticipated plasticity to SGs, which adapt their composition and function to cell growth activity, reflecting the ability of cells to adjust their stress response to their proliferation state and energy demands.

## Results

### TRAPP redistributes to SGs in response to different stress stimuli

To investigate the involvement of TRAPPC2 in the stress response, we exposed HeLa cells (Fig 1A), chondrocytes, fibroblasts or U2OS cells (Fig EV1A) to sodium arsenite (SA), a treatment that induces oxidative stress. SA treatment led to dissociation of TRAPPC2 from ERES, with which it associates under steady-state conditions (Venditti *et al*, 2012), with a complete relocation to roundish structures. Since oxidative stress is known to lead to the formation of stress granules (SGs; Anderson & Kedersha, 2002), we considered the possibility that these TRAPPC2-positive structures might be SGs. Indeed, co-labeling with an anti-eIF3 antibody, a canonical SG marker (Aulas *et al*, 2017), showed the co-localization of TRAPPC2 with eIF3 after SA treatment (Fig 1A). Interestingly, two different

disease-associated mutant forms of TRAPPC2 (D47Y, R90X; Choi *et al*, 2009; Venditti *et al*, 2012) exhibited reduced or no association with SGs, respectively (Fig EV1B).

Other components of the TRAPP complex, such as TRAPPC1, TRAPPC3, TRAPPC9 (a TRAPP-II-specific component) and TRAPPC8 (a TRAPP-III-specific component), were also recruited to SGs after SA treatment (Fig 1A), thus indicating that both TRAPP-II and TRAPP-III complexes can associate with SGs.

TRAPP recruitment to SGs also occurs in response to heat shock (Fig EV1C). In addition, TRAPP components associate with SGs in yeast cells exposed to heat stress (Fig EV1D, and Movies EV1 and EV2), thus suggesting that this is a conserved process in evolution. Of note, the association of TRAPP with SGs is fully reversible after stress removal (Fig EV1E).

We studied the kinetics of TRAPPC2 redistribution to SGs. The appearance of eIF3-positive SGs occurred 7 min after SA treatment (Fig 1B), while TRAPPC2 re-localization to SGs began 15 min after exposure to stress and gradually increased over time, with massive recruitment occurring 60 min after treatment, thus lagging behind the initial assembly of SGs (Fig 1B and B').

We observed that oxidative stress did not affect the overall integrity of the TRAPP complexes (both TRAPP-II and TRAPP-III), as analyzed by gel filtration (Fig EV1F).

It appears that TRAPPC2 exerts a pivotal role since TRAPPC2 depletion significantly reduced the recruitment of both TRAPP complexes to SGs (Fig 1C), as indicated by reduced TRAPPC8 and TRAPPC9 in SGs. By contrast, depletion of TRAPPC4, TRAPPC8, or TRAPPC9 did not significantly affect the recruitment of TRAPPC2 (Fig 1C).

To investigate the mechanisms underlying the recruitment of TRAPPC2 to SGs, we performed a proteomics analysis of the TRAPPC2 interactors both under steady-state conditions and after SA treatment (see Materials and Methods). This analysis (Figs 1D and EV1G, and Dataset EV1) confirmed known TRAPPC2 interactors (e.g., TRAPP complex components, CLIC1, and ENO1) and revealed the presence of many RNA binding proteins (RBPs), including those with a central role in the assembly of SGs (Jain *et al*, 2016). Interestingly, while some of these RBPs were found among the TRAPPC2 interactors at steady state, most of them were significantly enriched among TRAPPC2 interactors upon SA exposure. These findings suggested that, as described for other components of SGs, TRAPPC2 may be recruited to growing SGs by a piggyback mechanism (Anderson & Kedersha, 2008), i.e., via the interaction with RBPs that are components of SGs. Finally, as some of the known

### Figure 1. The TRAPP complex is recruited to stress granules.

- A Localization of TRAPP complex components after sodium arsenite (SA) treatment in HeLa cells treated with 300  $\mu$ M SA for 30 min. Fluorescence microscopy of fixed cells using antibodies against TRAPPC2 and eIF3 (to label SGs) at steady state and after SA treatment (top two rows). Other panels show localization of GFP-TRAPPC3 and endogenous TRAPPC1 to eIF3-labeled SGs and of endogenous TRAPPC9 and TRAPPC8 to G3BP-labeled SGs. DAPI (blue). Scale bar, 10  $\mu$ m.
- B Representative images of a time course analysis of TRAPPC2 redistribution to SGs. Cells were treated as in (A). The graph (B') shows quantification of TRAPPC2 localization at SGs over time as the ratio between TRAPPC2 (mean fluorescence intensity) in SG puncta and cytosolic TRAPPC2. Mean  $\pm$  s.e.m.  $n = 50$  cells per experiment,  $N = 3$ . Scale bar, 10  $\mu$ m.
- C Analysis of TRAPPC2 (green), TRAPPC8 (blue), and TRAPPC9 (orange) localization at SGs upon TRAPPC2, TRAPPC4, TRAPPC8, and TRAPPC9 depletion. Mean  $\pm$  s.e.m.  $n > 100$ . \* $P < 0.05$ ; ns: not significant, one-way ANOVA with Dunnett's multiple comparison test.
- D Schematic representation of MS/MS analysis of TRAPPC2 interactors. In addition to the TRAPP components and known TRAPPC2 interactors, 53 RNA binding proteins known to associate with SGs were co-IP with TRAPPC2. Proteins that associate with TRAPPC2 only upon SA treatment are highlighted in red.
- E Analysis of TRAPPC2 localization at SGs upon CLIC1, CRYAB, and ENO1 depletion. Mean  $\pm$  s.e.m.  $n > 100$ . \*\*\*\* $P < 0.0001$ ; ns: not significant, one-way ANOVA with Dunnett's multiple comparison test.

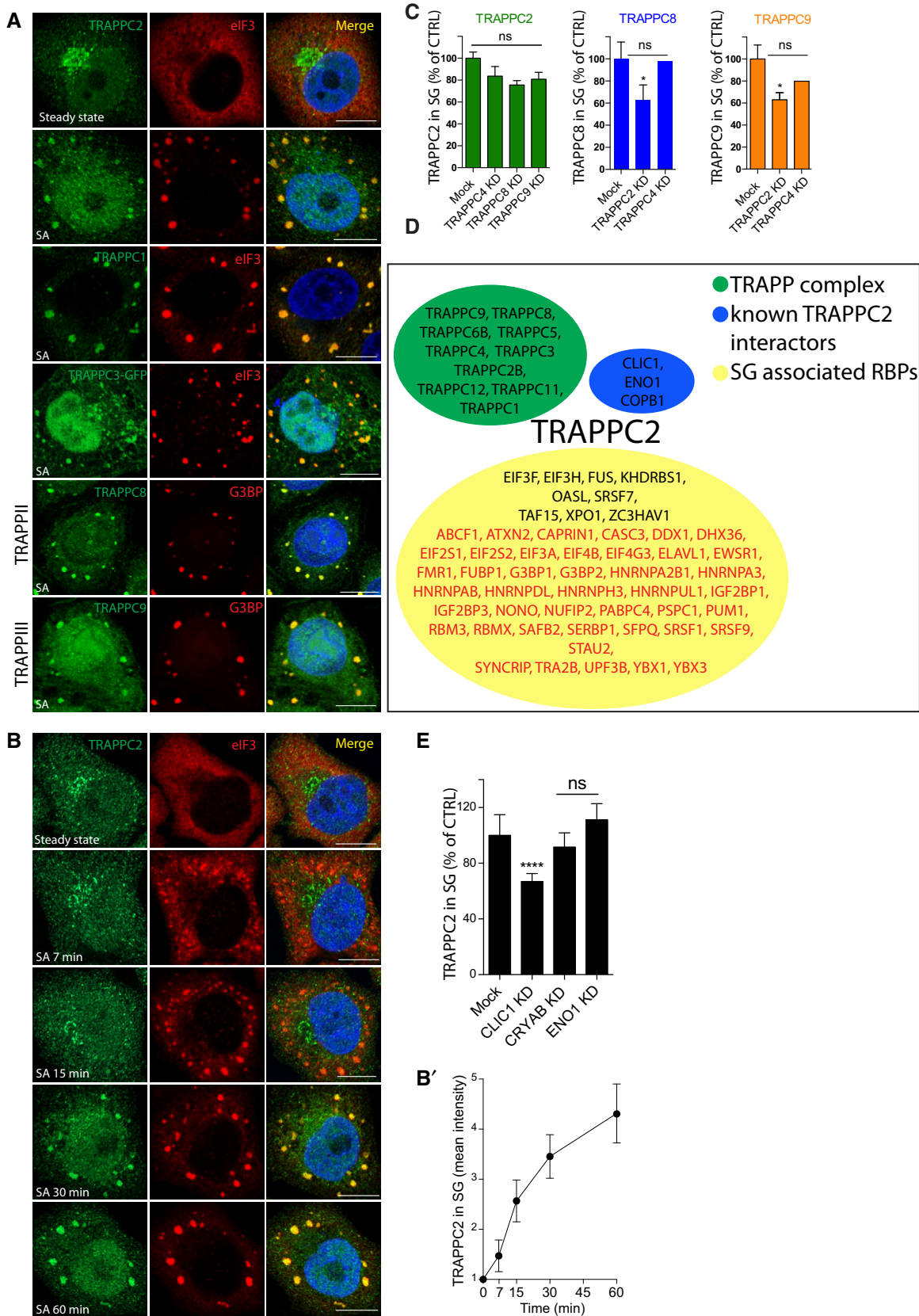


Figure 1.

interactors of TRAPPC2, such as CLIC1, ENO1, and CRYAB, have been described as associating with SGs (Jain *et al*, 2016), we investigated whether they were involved in TRAPPC2 recruitment and found that CLIC1, but not ENO1 or CRYAB, is involved in TRAPPC2 recruitment to SGs (Fig 1E).

Altogether, these results led us to conclude that following stress the TRAPP complexes, through interaction of TRAPPC2 with multiple SG components, associate with SGs.

### TRAPPC2 is required for recruiting COPII to SGs

The translocation of TRAPP to SGs prompted us to investigate whether other components of membrane trafficking machineries behaved similarly. We screened different coat complex components (COPI, COPII, clathrin adaptors, clathrin), and other cytosolic proteins associated with the exocytic and endocytic pathways. Out of the 28 proteins tested, only components of the inner layer of the COPII coat, Sec24 (in its four isoforms) and Sec23, but none of the others (Figs 2A and B, and EV2A–D) associated with SGs. Notably, the recruitment of Sec24 to SGs occurred with kinetics similar to those of the TRAPP complex (Fig 2B) and induced a marked reduction of Sec24 associated with ERES (Fig 2C).

Since TRAPP and COPII are known to interact and TRAPP is recruited to ERES in a Sar1- and COPII-dependent manner (Lord *et al*, 2011; Venditti *et al*, 2012), we asked whether COPII and TRAPP recruitment to SGs is interdependent. The depletion of the COPII inner layer proteins Sec23 and Sec24 had no impact on the recruitment of the TRAPP complex to SGs (Fig 2D and E, Appendix Fig S1) while the depletion of the entire TRAPP complex (by KD of TRAPPC3, which destabilizes the entire complex) or of the TRAPPC2 subunit (by KD of TRAPPC2 or by TRAPPC2 KO via CRISPR-CAS9) abrogated the recruitment of COPII components to SGs (Fig 2F and G). These results indicated that the TRAPP complex, through its component TRAPPC2, drives the recruitment of COPII to SGs formed in response to acute oxidative stress.

It is worth mentioning that COPII components have been reported to partition in membrane-less bodies called “Sec bodies” in *Drosophila* S2 cells (Zacharogianni *et al*, 2014). Sec bodies, which are distinct from SGs as they are devoid of RBPs, form exclusively in response to prolonged amino acid starvation and not in response to acute oxidative stress (Zacharogianni *et al*, 2014). The formation

of Sec bodies in mammalian cells has remained unclear (Zacharogianni *et al*, 2014). In fact, we found that COPII components (Sec24C and Sec31A) do not form Sec bodies as they remain even more associated with ERES in amino acid-starved mammalian cells (Fig EV3A and B). We also found that Sec16, which is required for the formation of Sec bodies and SGs in response to amino acid starvation in *Drosophila* S2 cells (Zacharogianni *et al*, 2014; Aguilera-Gomez *et al*, 2017), neither significantly associates with SGs formed in response to stress in mammalian cells (Fig EV3C and D) nor is it required for the recruitment of COPII to these SGs (Fig EV3E and F).

Altogether these results indicate that COPII components can undergo two distinct phase separation events: They can associate in a TRAPP-dependent fashion with SGs in response to acute stress in mammalian cells (this report) and they can assemble in a Sec16-dependent manner in “Sec bodies” in *Drosophila* S2 cells in response to amino acid starvation (Zacharogianni *et al*, 2014). Interestingly, these two distinct phase separation events lead to different functional consequences (see below).

We then investigated the nature of the association of COPII with SGs since the COPII coat cycles in a very dynamic fashion at ERES (D’Arcangelo *et al*, 2013). To this end, we permeabilized living cells (Kapetanovich *et al*, 2005) at steady state and upon stress induction. Treatment with digitonin forms pores at the plasma membrane that allows the exit of the cytosolic content into the extracellular space. Under these conditions, we found that the COPII pool recruited to SGs is less dynamic than the pool cycling at the ERES, since COPII remained associated with SGs in permeabilized cells exposed to stress while the COPII pool cycling at the ERES was completely lost upon permeabilization of unstressed cells (Fig 3A). We then assessed the possible interplay between the COPII fraction at ERES and the pool that eventually relocates to SGs. We asked whether changes in the association of COPII at the ERES could have an impact on the recruitment of COPII to SGs. To this end, we stabilized COPII and TRAPP at ERES by expressing either a constitutively active GTP-bound Sar1 mutant (Sar1-H79G) or decreasing the rate of GTP hydrolysis on Sar1 by depleting Sec31, which is a co-GAP that potentiates by an order of magnitude the Sar1 GAP activity of Sec23–24 (Bi *et al*, 2007). Under both conditions, COPII and TRAPP were more tightly associated with ERES, while their translocation to SGs upon exposure to stress was significantly reduced (Fig 3B–D). Thus, COPII/TRAPP recruitment to SGs is commensurate with the

### Figure 2. TRAPPC2 is required for Sec23/24 re-localization to SGs.

- A HeLa cells, untreated or treated with SA, were fixed and visualized by fluorescence microscopy using anti-Sec24C Ab, anti-eIF3 Ab, and DAPI (blue).
- B Quantification of Sec24C redistribution to SGs over time after SA treatment [the ratio between Sec24C (mean fluorescence intensity) in SG puncta and cytosolic Sec24C]. Mean  $\pm$  s.e.m.  $n = 50$  cells per experiment,  $N = 3$ .
- C Quantification of residual Sec24C in ERES after SA treatment. The data are expressed as percentage of steady-state values (CTRL). Mean  $\pm$  s.e.m.  $n = 100$  cells per experiment,  $N = 3$ .
- D Representative images of TRAPPC2 localization in Sec23AB-KD and Sec24ABCD-KD cells treated with SA. Cells were fixed and visualized by fluorescence microscopy using anti-TRAPPC2 Ab, anti-G3BP Ab (to label SGs), and DAPI (blue).
- E Quantification of TRAPPC2 redistribution to SGs after KD of the indicated Sec23 and Sec24 combinations, calculated as the ratio between TRAPPC2 (mean intensity) in SG puncta and cytosolic TRAPPC2 and expressed as % of CTRL. Mean  $\pm$  s.e.m.,  $n = 40$ –60 cells per experiment,  $N = 3$ . ns: not significant, One-way ANOVA with Dunnett’s multiple comparison test.
- F Representative images of Sec24C localization at SGs (stained for G3BP) in TRAPPC3-KD and TRAPPC2-KD cells treated with SA. Depletion of the entire TRAPP complex (via TRAPPC3 depletion) or of only TRAPPC2 reduces Sec24C recruitment. Graph, quantification of Sec24C at SGs, calculated as in (E). Mean  $\pm$  s.e.m.,  $n = 40$ –60 cells per experiment,  $N = 3$ . \*\*\*\* $P < 0.0001$ , One-way ANOVA with Dunnett’s multiple comparison test.
- G Representative images of Sec24C localization at SGs (stained for G3BP) in TRAPPC2-KO cells treated with SA.

Data information: (A, D, F, G) Scale bars, 10  $\mu$ m.

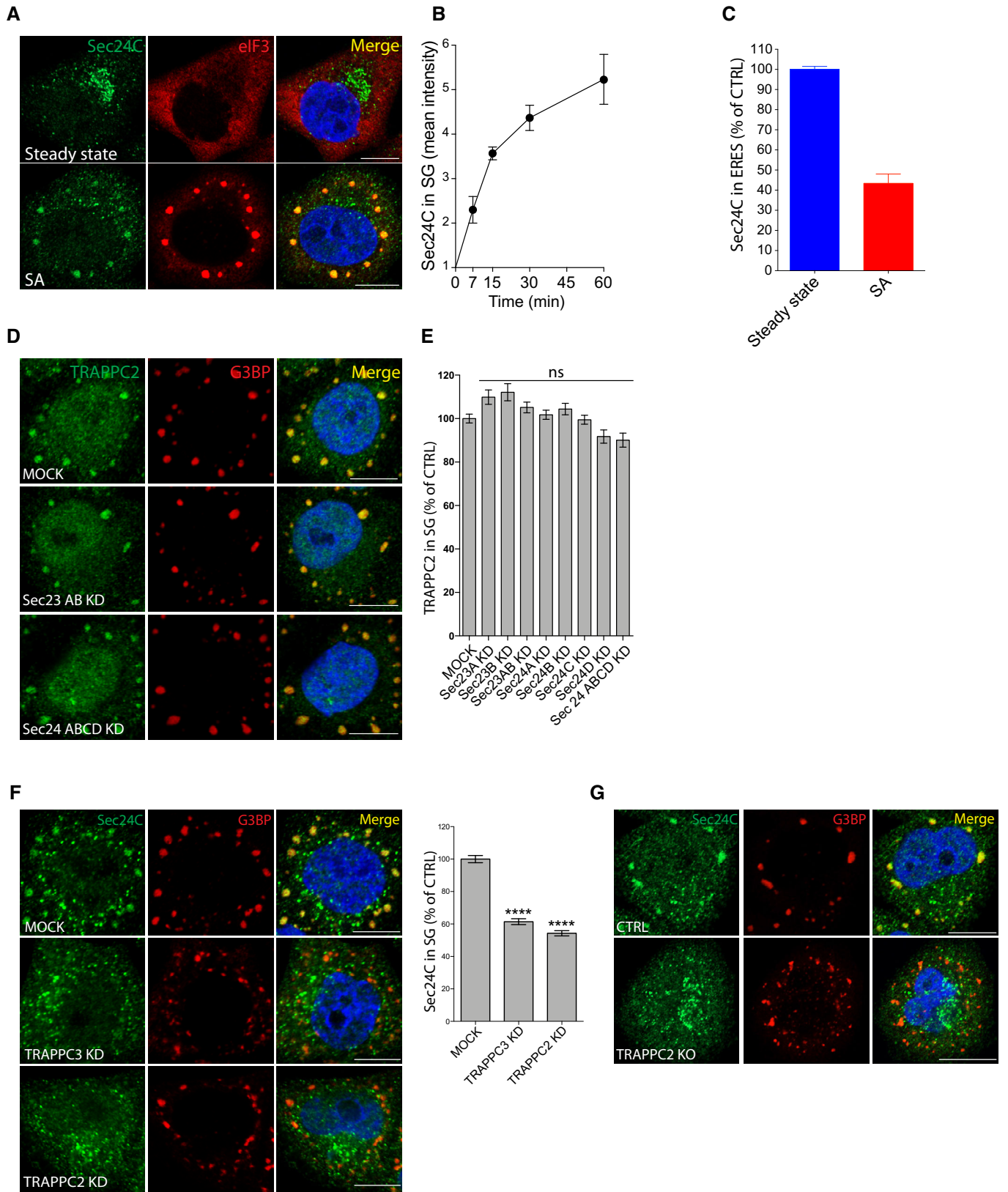


Figure 2.

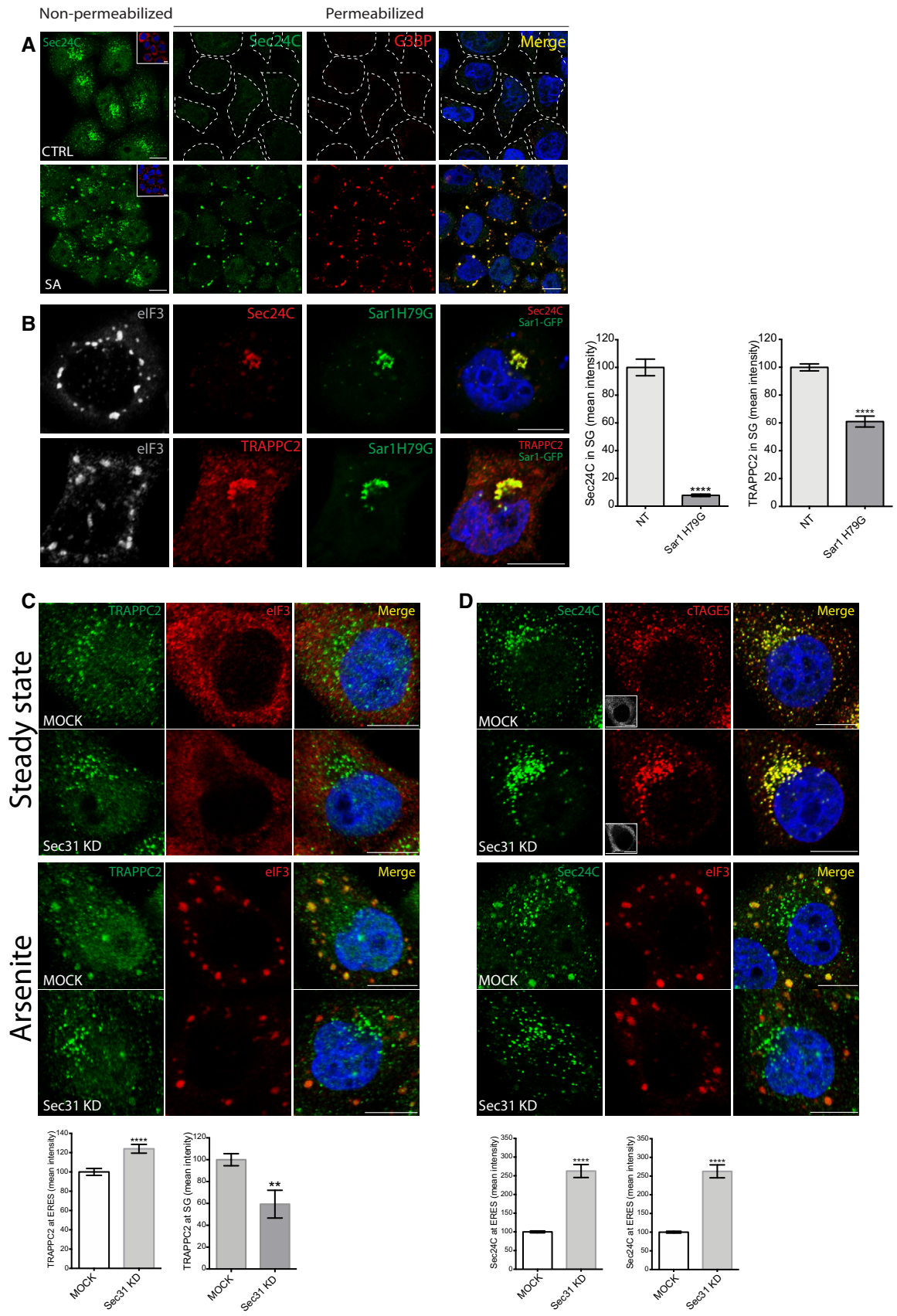


Figure 3.

**Figure 3. Comparison and relationships between the ERES-associated and the SG-associated pools of TRAPP and COPII.**

- A TRAPP and COPII associate more stably with SGs than with ERES. The membrane association of Sec24C was evaluated in non-permeabilized or permeabilized cells with or without SA treatment, as indicated. G3BP was used as an SG marker. Left panel insets, G3BP staining in non-permeabilized cells. Dashed white lines show the outline of permeabilized SA-untreated cells. Blue, DAPI.
- B Stabilizing TRAPP and COPII at the ERES prevents their re-localization to SGs. HeLa cells overexpressing GFP-Sar1H79G were treated with SA and immunostained for Sec24C, TRAPPC2, and eIF3, as indicated. Blue, DAPI. Graphs show quantification of Sec24C or TRAPPC2 at SGs in GFP-Sar1H79G-expressing cells. Data are the ratio between Sec24C or TRAPPC2 mean intensity in SG puncta and Sec24C or TRAPPC2 mean intensity at ERES, expressed as a percentage of the non-transfected (NT) cells. Mean  $\pm$  s.e.m.  $n = 60$ – $70$ , three independent experiments. \*\*\*\* $P < 0.0001$ , Student's unpaired two-tailed  $t$ -test.
- C Effect of Sec31A depletion on TRAPPC2 recruitment to SGs. Cells were mock-treated or KD for Sec31, treated with SA, and then immunostained for TRAPPC2 and eIF3 as indicated. Graphs, quantification of TRAPPC2 at ERES and SGs after SA treatment. Mean  $\pm$  s.e.m., one representative experiment;  $n = 60$ – $80$ . \*\* $P < 0.001$ , \*\*\*\* $P < 0.0001$ , Student's unpaired two-tailed  $t$ -test.
- D Effect of Sec31A depletion on Sec24C recruitment to SGs. Cells were mock-treated or KD for Sec31 and then immunostained for Sec24C and cTAGE5 (to stain ERES, top panels) and for eIF3 (bottom panels). Insets show eIF3. Graphs, quantification of Sec24C at ERES and in SGs after SA treatment.  $n = 80$ . \*\*\*\* $P < 0.0001$ , Student's unpaired two-tailed  $t$ -test.
- Data information; (A–D) Scale bars, 10  $\mu$ m.

rate of their association at the ERES indicating that it is the cytosolic pool of COPII generated through the fast cycling at ERES that is recruited to SGs upon stress.

### The association of TRAPP/COPII with SGs is under the control of CDK1/2

To dissect the regulation of TRAPP/COPII recruitment to SGs, we screened a library of kinase inhibitors for their ability to affect the re-localization of COPII to SGs. HeLa cells were pre-treated with kinase inhibitors for 150 min and then exposed to SA for a further 30 min in the continuous presence of the inhibitors. Out of the 273 inhibitors tested, 194 had no effect on SG formation or on COPII recruitment, 13 were generally toxic (65% mortality) at the tested concentrations, one (AZD4547) affected the formation of SGs, while the remaining 32 specifically inhibited (by at least 35%) the association of Sec24C with SGs without affecting SG formation (Fig 4A). Enrichment analysis on this last group of inhibitors highlighted that CDK inhibitors were the most represented class (Fig 4B). Western blot analysis confirmed that CDK activity was impaired in cells treated with the CDK inhibitors (Fig 4C). In addition, we observed that there is an increase in CDK activity in SA-treated cells that was sensitive to CDK inhibitors (Fig 4C).

The CDK protein kinase family is composed of 21 members (Malumbres, 2014), and available inhibitors have limited selectivity (Asghar *et al*, 2015). To identify which specific CDK might be involved in Sec24C recruitment, we compared the potency of selected CDK inhibitors (flavopiridol hydrochloride, SNS-032, dinaciclib, AT7519, PHA-793887, ADZ5438, JNJ-7706621, PHA-767491, BMS-265246, PHA-848125, roscovitine, palbociclib, BS-181HCl) in the Sec24C recruitment assay with their ability to inhibit different CDK isoforms, as described by Selleckchem (<https://www.selleckchem.com/CDK.html>). This analysis revealed that CDK1 and 2 were those commonly targeted by the inhibitors that most potently affected Sec24C recruitment to SGs (Fig 4D), strongly suggesting that CDK1/2 are the most likely CDKs controlling COPII recruitment to SGs. This was confirmed by the observation that titrating the expression of CDK1 and CDK2 by siRNA inhibited COPII recruitment to SGs (Fig 4E, Appendix Fig S1). The three best hits (flavopiridol, dinaciclib, SNS032, Fig 4D and F) were assayed using a dose–response analysis and were found to be effective at concentrations as low as 100 nM (Fig 4G). As a negative control, the specific CDK7 inhibitor (BS-181HCl) was ineffective, even at the highest concentration tested (Fig 4G).

Since COPII recruitment to SGs is driven by TRAPPC2 recruitment (Fig 2F), we predicted that CDK1/2 inhibitors would also inhibit TRAPP recruitment. In line with our expectations, TRAPPC2 re-localization to SGs was reduced in cells treated with CDK1/2 inhibitors (Fig 4H).

Altogether, these results indicate that a signaling pathway involving CDK1/2 controls the redistribution of TRAPP and COPII from ERES to SGs. To dissect the mechanisms underlying this regulation, we took into consideration two possible non-exclusive scenarios. CDK1/2 may control the membrane/cytosol cycle of TRAPP-COPII (which in turn determines the extent of their recruitment to SGs, Fig 3B and D) and/or they may interfere with the association of TRAPP-COPII with SGs.

Indeed, we found that CDK inhibitors stabilize TRAPP and COPII on ERES membranes (even in unstressed cells, Fig 5A), thus increasing the membrane-associated pool and decreasing the cytosolic pool (Fig 5B and C), which is the one available for SG translocation.

We then assessed whether CDK can control the association of TRAPP/COPII with SGs by acting on SG components that may pilot TRAPP to SGs. The heterogeneous nuclear ribonucleoprotein K (hnRNPK) is a ubiquitous RBP that has been implicated in proliferation, differentiation, apoptosis, DNA damage repair, and stress response (Moujalled *et al*, 2015). hnRNPK is highly controlled via post-translation modifications, including phosphorylation by CDK1-2 at S216 and/or S284. It has been shown that CDK-mediated phosphorylation regulates the association of hnRNPK with TDP-43-positive SGs as well as their formation (Moujalled *et al*, 2015). We thus assessed whether hnRNPK is involved in TRAPPC2 recruitment to SGs, which might contribute to the observed CDK sensitivity. We found that hnRNPK associates with SA-induced SGs in a CDK-dependent manner (Fig 5D) that TRAPPC2 interacts with hnRNPK (Fig 5E) and that, more importantly, hnRNPK is required for TRAPP and COPII recruitment to SGs (Fig 5F–H).

Altogether, the above results indicate that CDK1/2 control the translocation of TRAPP/COPII to SGs by concurrently regulating the rate of their association with ERES and, through hnRNPK, their recruitment to SGs.

### The recruitment of TRAPP and COPII to SGs occurs in actively proliferating cells

The observation that the recruitment of TRAPP and COPII to SGs is under control of CDK1/2 suggested that it could be linked to cell

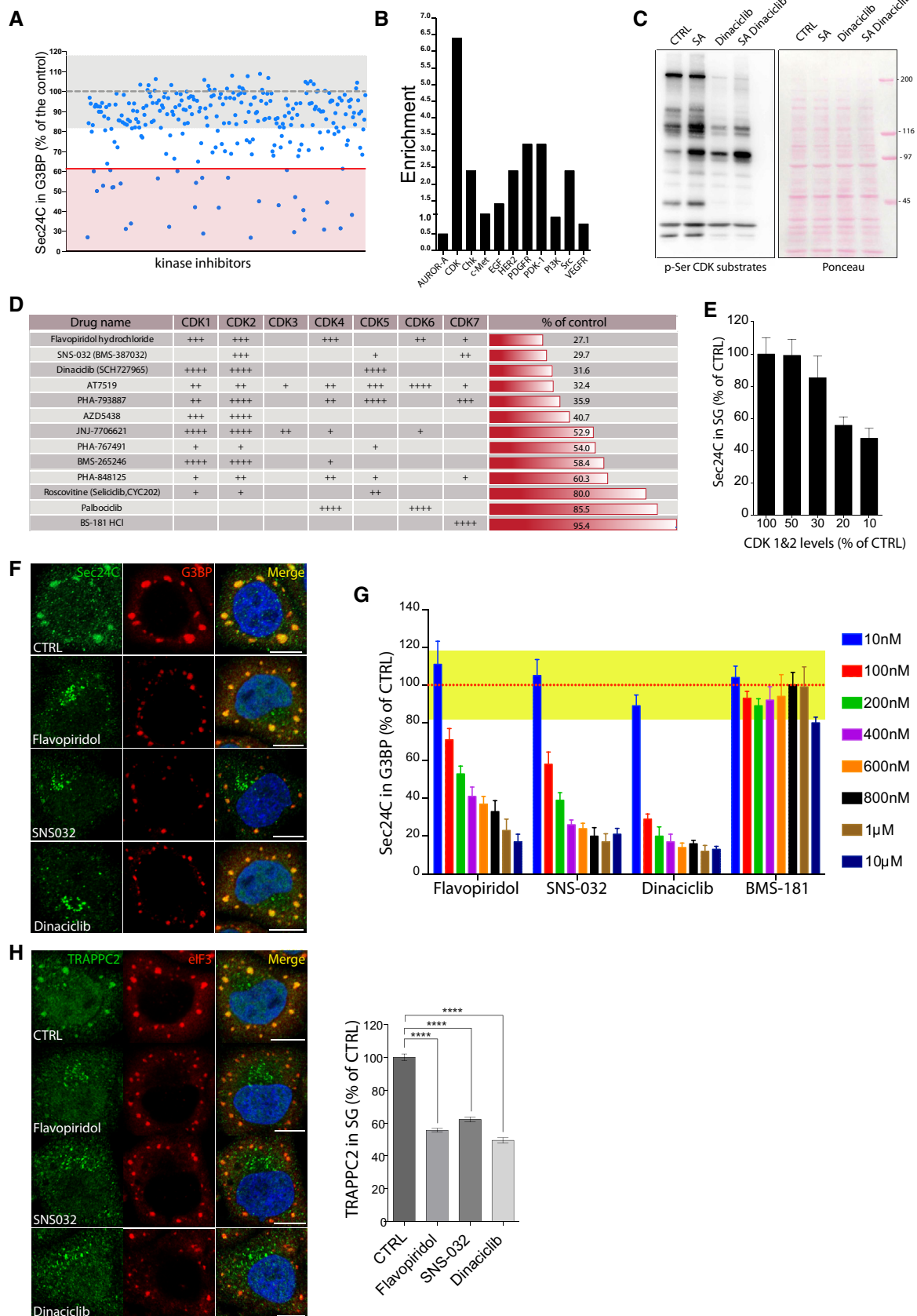


Figure 4.

**Figure 4. The association of TRAPP with SGs is under control of CDK1/2.**

- A Cells were treated with 273 kinase inhibitors (10  $\mu$ M) from the Selleckchem library and with SA, and Sec24C localization in G3BP puncta (% of total G3BP area) was analyzed by automated microscopy as described in Materials and Methods under high-content screening and is reported as a percentage of the control (cells treated with SA alone). Gray dashed line, mean of control; gray box, control standard deviation ( $\pm 18.2\%$ ); red line, threshold of positive hits; red box: positive hits.
- B Enrichment analysis of the positive hits; for each class of inhibitor, the enrichment (in percentage) of compounds falling into positive hits and the enrichment (in percentage) in the total number of compounds was calculated and expressed as a ratio.
- C Evaluation of CDK kinase activity upon SA treatment. Western blot analysis of phosphoSer-CDK substrates in control, SA (300  $\mu$ M, 30 min), dinaciclib (10  $\mu$ M, 180 min), and SA+dinaciclib (150 min dinaciclib and 30 min SA). CDKs are hyperactivated upon oxidative stress, and this activation is partially prevented upon CDK inhibition. Left, Western blot, right: Ponceau was used as loading control. Image, one representative experiment out of three independent replicates.
- D Drug specificity from high (++++) to low (+) of the different CDKs as described by Selleckchem, and Sec24C recruitment to SGs as a percentage of control.
- E Analysis of Sec24C recruitment to SGs in control and CDK1 + 2-KD HeLa cells. Different levels of CDK1 + 2 KD were achieved by transfecting cells with different amounts of siRNA for different times (2 nM 24 h; 5 nM 24 h; 5 nM 48 h; 20 nM 48 h) to give 50, 30, 20, and 10%, respectively, of the CDK1 + 2 levels in the control. CDK1 + 2 levels measured by qRT-PCR and Sec24C recruitment to SGs were evaluated from parallel cultures. Sec24C recruitment to SGs was performed by automated microscopy as described in (A) and is expressed as a percentage of mock (CTRL, set at 100%)  $\pm$  s.d.  $N = 8$ .
- F Representative images of HeLa cells treated with the three best hits (flavopiridol, SNS-032, dinaciclib; 1  $\mu$ M 150 min) and then exposed to SA (300  $\mu$ M, 30 min), followed by immunostaining for Sec24C and G3BP. Scale bar, 10  $\mu$ m.
- G HeLa cells were treated with flavopiridol, SNS-032, or dinaciclib for 150 min at the indicated concentrations, subsequently treated with SA (300  $\mu$ M, 30 min), and then immunostained for Sec24C and G3BP and imaged by OPERA. BS-181, a specific CDK7 inhibitor, was used as negative control. Sec24C localization to SGs is expressed as a percentage of the control (cells treated with SA alone). Dashed red line, mean of control; yellow box, standard deviation of control ( $\pm 9.8\%$ ),  $N = 12$ .
- H Cells were treated as in (G) and immunostained for TRAPPC2 and eIF3. Scale bar, 10  $\mu$ m. The graph shows the quantification of TRAPPC2 localization in SG puncta (mean intensity). Data are mean  $\pm$  s.e.m. expressed as a percentage of TRAPPC2 signal in SGs after flavopiridol, SNS-032, or dinaciclib treatment compared to the control (cells treated with SA alone).  $N = 3$ , three independent experiments,  $n = 60$ –80 cells per experiment. \*\*\*\* $P < 0.0001$ , One-way ANOVA with Dunnett's multiple comparison test.

Source data are available online for this figure.

proliferation. We explored this possibility by decreasing the cell proliferation rate in diverse and independent ways.

First, cells were subjected to prolonged nutrient starvation (HBSS for 8 h) and then were exposed to SA for 30 min. Under these conditions, which inhibited cell proliferation, TRAPP/COPII association with SGs was reduced (Fig 6A and B).

Second, HeLa cells were seeded at different confluency and then treated with SA for 30 min. Strikingly, the extent of confluency was inversely related to the extent of TRAPP/COPII association with SGs and to the degree of proliferation (Fig 6C).

Third, we monitored the recruitment of TRAPP/COPII to SGs in podocyte cells expressing a temperature-sensitive LTA-SV40 that actively proliferate at the permissive temperature of 33°C but arrest proliferation and differentiate at the restrictive temperature of 37°C (Saleem *et al*, 2002; Fig 6D and E). While TRAPP and COPII associate with SGs in undifferentiated podocytes in response to stress, this association was reduced in differentiated podocytes (Fig 6E). Of note, the proliferation to differentiation switch, as described (Saurus *et al*, 2016), is also accompanied by a decline in CDK activity (Fig 6F and G).

Altogether, these data indicate that the association of COPII and TRAPP with SGs occurs only in proliferating cells and requires active CDK1/2 signaling.

### The TRAPP complex imposes SG size, composition, and function

The identification of TRAPP as a component of SGs led us to ask whether it could play any role in the assembly and function of SGs themselves. Indeed, we observed that depleting the entire TRAPP complex or only TRAPPC2 (through siRNA-mediated depletion) decreased the size of SGs (Figs 2F and 7A). Microinjection of a TRAPPC3-blocking Ab (Yu *et al*, 2006; Venditti *et al*, 2012) had a similar effect (Fig 7B). Moreover, a smaller size of SGs was also observed upon treatment with CDK1/2 inhibitors, which prevents TRAPP translocation to SGs (Fig 4F and H). Under all of the above

conditions, the size of the SGs recalls that of “immature SGs” (Wheeler *et al*, 2016).

In fact, the processes that lead to SG nucleation, i.e., shut-down of protein synthesis or phosphorylation of eIF2 $\alpha$  induced by oxidative stress, were not affected by TRAPP depletion (Fig EV4A and B). Instead, the successive increase in size of the nucleated SGs (i.e., SG maturation) was impaired in TRAPP-depleted cells, consistent with our observation that TRAPP is recruited after the initial formation of SGs (Fig 1D) and occupies an outer position in the SGs (Fig 7C). A feature of SG maturation is the acquisition of an array of signaling molecules (which can be either hyperactivated or deactivated) to drive the pro-survival program (Franzmann & Alberti, 2019). This is the case of Raptor, which controls the energy sensor mTORC1 and the kinase RACK1 (Arimoto *et al*, 2008; Thedieck *et al*, 2013; Wippich *et al*, 2013). To evaluate whether the absence of TRAPP could affect SG maturation and/or signaling function by interfering with the recruitment of these proteins, we checked the localization of Raptor (Fig 7D) and RACK1 (Fig 7E) in TRAPP-depleted cells subjected to oxidative stress. We observed that the amount of these signaling proteins sequestered to SGs was strongly reduced by TRAPP depletion. We next wondered whether the TRAPP dependence of RACK1 and Raptor association with SGs might be due to a physical interaction and we found that this is indeed the case as Raptor and Rack1 can be co-immunoprecipitated with TRAPP using TRAPPC2 as bait (Fig 7F and G). Consistent with a role for TRAPP in mediating the SG recruitment of RACK1 and Raptor, these signaling proteins failed to associate with SGs under conditions of CDK inhibition where TRAPP does not associate with SGs (Fig 7H and I).

SGs are part of a pro-survival program that aims to save energy to cope with stress insults. Interfering with this program by impairing SG formation sensitizes cells to apoptosis (Takahashi *et al*, 2013). We thus assayed stress resistance in TRAPPC2-depleted cells where the maturation of SGs was impaired and found that they were more susceptible to apoptosis induced by oxidative stress (Fig 7J).

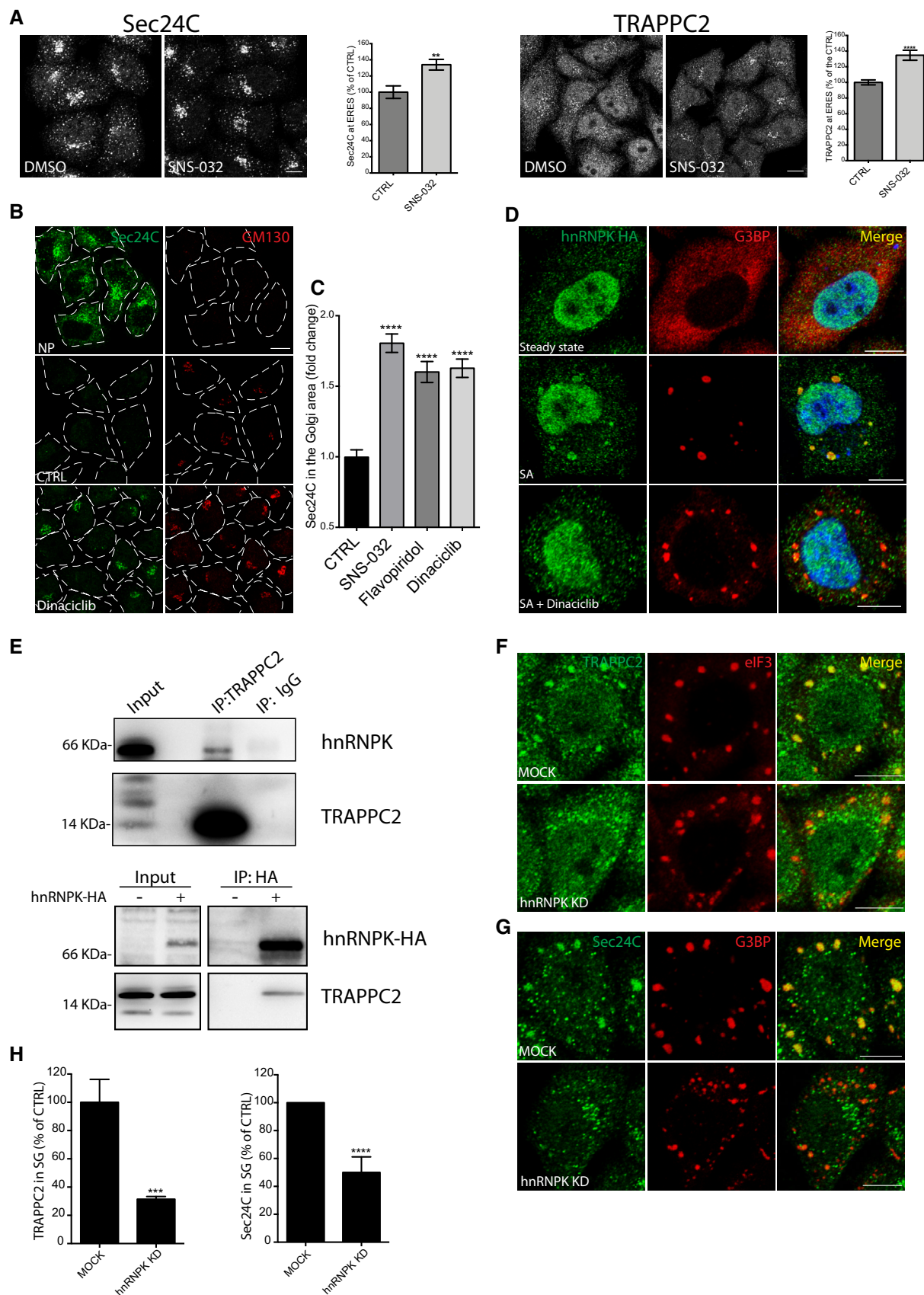


Figure 5.

**Figure 5. CDK1/2 modulate the COPII cycle at ERES.**

- A Immunofluorescence images of Sec24C and TRAPPC2 in vehicle-treated and SNS-032-treated (1  $\mu$ M, 3 h) cells. Graphs show the quantification of Sec24C and TRAPPC2 at ERES (mean intensity) normalized in SNS-032-treated cells relative to vehicle-treated cells (set as 100%). Mean  $\pm$  s.e.m. of three independent experiments. \*\* $P$  < 0.05, \*\*\*\* $P$  < 0.0001, Student's unpaired two-tailed  $t$ -test.
- B HeLa cells were treated with dinaciclib (1  $\mu$ M, 3 h) and permeabilized or not with digitonin as described in Materials and Methods. A GM130 antibody was added to the buffer of living cells to monitor permeabilization efficiency. Upper panels, non-permeabilized (NP) control cells; middle panels, permeabilized control cells; lower panels, permeabilized dinaciclib-treated cells.
- C Quantification of Sec24C membrane association after CDK inhibitor treatment. Digitonin-permeabilized cells treated with vehicle (CTRL) or the indicated CDK inhibitor (1  $\mu$ M, 3 h) were immunostained for Sec24C. The mean intensity of Sec24C in the perinuclear area normalized for the cytosolic Sec24C signal in drug-treated cells is expressed as fold change compared to the control;  $n$  = 60–80; mean  $\pm$  s.e.m. of three independent experiments \*\*\*\* $P$  < 0.0001, one-way ANOVA with Dunnett's multiple comparison test.
- D HeLa cells transfected with HA-hnRNPk were left untreated (steady state) or treated with SA (300  $\mu$ M, 30 min) or SA+dinaciclib (10  $\mu$ M, 150 min) and then immunostained with anti-HA and anti-G3BP antibodies.
- E TRAPPC2 interacts with hnRNPk. (Top) SDS-PAGE and Western blot analysis of endogenous hnRNPk after immunoprecipitation with an anti-TRAPPC2 Ab or IgG, and (bottom) after immunoprecipitation with an anti-HA Ab from cells transfected (+) or not (–) with hnRNPk-HA detected with the indicated antibodies.
- F Mock or hnRNPk KD cells treated with SA were immunostained for TRAPPC2 and eIF3.
- G Mock or hnRNPk KD cells treated with SA were immunostained for Sec24C and G3BP.
- H Graphs show quantification of TRAPPC2 and Sec24C redistribution to SGs in mock-treated (CTRL) and hnRNPk KD cells.  $n$  > 100,  $N$  = 3 mean  $\pm$  s.d. \*\*\* $P$  < 0.001, \*\*\*\* $P$  < 0.0001, Student's unpaired two-tailed  $t$ -test.

Data information: (A, B, D, F, G) Scale bars, 10  $\mu$ m.

Source data are available online for this figure.

Finally, the observation that CDK inhibitors, which also impair TRAPP recruitment and maturation of SGs, significantly sensitized cells to cell death upon SA treatment (Fig 7K) is consistent with the idea that TRAPP might confer anti-apoptotic functions to SGs, although additional anti-apoptotic effects of these compounds cannot be excluded.

### The recruitment of TRAPP and COPII to SGs impairs ER export of newly synthesized cargoes and induces the fragmentation of the Golgi complex

We finally investigated the functional relevance of the recruitment of TRAPP/COPII to SGs by analyzing its impact on the function and structure of the secretory pathway.

Initially, we tested whether the residual COPII coat associated with ERES after SA treatment, which was evaluated as 40% of control (Fig 2C), was capable of sustaining efficient ER export. We reduced COPII to comparable levels by the siRNA-mediated combined depletion of Sec24A, B, C, and D (Fig EV5A) and found that the export of newly synthesized proteins from the ER was significantly delayed in these cells (Fig EV5B).

We thus analyzed the ER export of newly synthesized cargo in cells exposed to oxidative stress, taking into consideration both endogenous and reporter cargo proteins, procollagen type I (PC-I; Venditti *et al*, 2012; Gorur *et al*, 2017), and VSVG, respectively (Fig 8A–D).

PC-I transport can be synchronized by temperature, being unfolded and blocked in the ER at 40°C while properly folded, assembled and exported from the ER, transported to the Golgi complex (GC), and secreted at 32°C (Mironov *et al*, 2001, and Materials and Methods). Human fibroblasts were incubated at 40°C, left untreated or treated with SA (Fig 8A). PC-I was blocked in the ER under both conditions (Fig 8A). Monitoring of PC-I transport after the shift to 32°C showed that while PC-I reaches the GC in untreated cells, it remains blocked in the ER in SA-treated cells (Fig 8A).

We then investigated to what extent the inhibition of cargo export from the ER induced by oxidative stress is dependent on

COPII/TRAPP depletion consequent to their sequestering onto SGs. To this end, we prevented the sequestering of COPII/TRAPP by impairing the formation of SGs themselves. To impair the formation of SGs, we used ISRIB, a compound that antagonises the effects of eIF2 $\alpha$  phosphorylation on translation and inhibits SG assembly (Sidrauski *et al*, 2015; Rabouw *et al*, 2019). In preliminary experiments, we checked the ability of ISRIB to impair SG formation under our experimental conditions and, in agreement with published reports (Rabouw *et al*, 2019), found that ISRIB completely abrogates SG assembly after 15-min SA treatment and delayed their appearance at later time points of treatment, thus significantly also impairing COPII sequestering to SGs (Fig 8B and C). To monitor the synchronized export of neosynthesized cargo, we followed the trafficking of VSVG-UVR8, which exits the ER in a UV light-inducible manner (Chen *et al*, 2013). After UV light induction, VSVG-UVR8 exited the ER and reached the Golgi in control cells, while its ER export was severely impaired in cells treated with SA under conditions permissive for SG formation, where COPII was massively recruited to SGs (Fig 8D). However, the inhibition of ER export of VSVG-UVR8 was largely prevented when the cells were exposed to similar oxidative stress but under conditions that impaired SG formation (i.e., when cells were pre-treated with ISRIB; Fig 8B–D and F).

Supporting the conclusion that the stress-induced sequestering of TRAPP and COPII to SGs mediates the impairment in ER export, we found that ER export was largely preserved in highly confluent cells (Fig EV5C), where TRAPP and COPII complexes are not re-localized to SGs upon SA treatment.

We next tested whether COPII and TRAPP maintain their functionality once released from SGs upon stress removal (Fig EV1D). Cells were treated with SA for 30 min, the SA was washed out, and cells were left to recover for 120 min in the presence of cycloheximide to prevent *de novo* synthesis of TRAPP and COPII components. Under these conditions, SGs were resolved, COPII returned to its native location (ERES/cytosol), and cells completely recovered their capability to transport cargo to the Golgi apparatus (Fig 8E and F). These data indicate that sequestration of COPII/TRAPP onto SGs

halts ER-to-Golgi trafficking while removal of the stress releases COPII/TRAPP and allows trafficking to resume.

COPII and TRAPP not only control ER export but are also needed to maintain the organization of the GC. In particular, the TRAPP complex acts as GEF for Rab1, a GTPase with a key role in the organization and function of the GC (Tisdale *et al*, 1992; Wilson *et al*, 1994). We monitored Golgi complex morphology in response to SA

by following the distribution of the early Golgi marker GM130. Strikingly, the GC starts to fragment after 30 min and completely redistributes throughout the cytoplasm after 60 min of SA treatment (Fig 9A). This time window overlaps with the progressive recruitment of the TRAPP complex onto SGs (Fig 1B). To assess whether the Golgi fragmentation induced by oxidative stress was due to sequestration of TRAPP/COPII onto SGs, we analyzed the

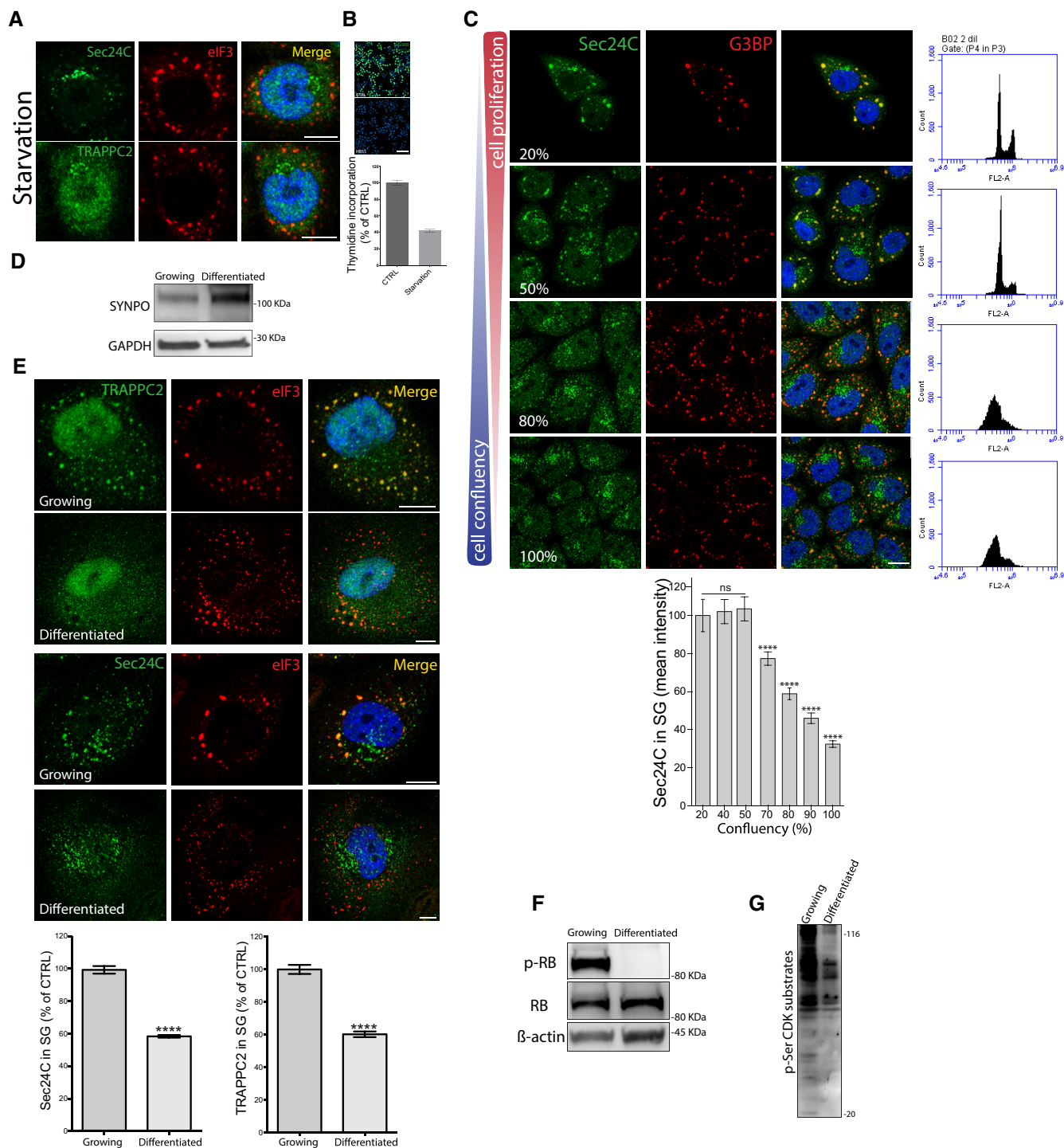


Figure 6.

**Figure 6. TRAPP and Sec23/24 migration to SGs depends on the proliferation state of cells.**

- A HeLa cells were starved for 8 h with HBSS and subsequently exposed to SA (30 min, 300  $\mu$ M), and immunostained for Sec24C or TRAPPC2 and eIF3. Scale bar 10  $\mu$ m.
- B Analysis of the proliferation status of the cells after 8-h starvation in HBSS. Top, representative images of starved and non-starved (CTRL) cells using EdU incorporation (see Materials and Methods). Scale bar, 100  $\mu$ m. Bottom, quantification of EdU incorporation in starved cells as a percentage of incorporation in control fed cells,  $N = 3$ , mean  $\pm$  s.d.
- C HeLa cells were seeded at different confluency, treated with SA, and stained for Sec24C and G3BP as an SG marker. Scale bar, 10  $\mu$ m. Flow cytometry (FACS) analysis (right panels) was performed to evaluate the distribution of cell cycle phases in HeLa cell populations seeded at different confluency. The graph shows quantification of Sec24C mean intensity in SG puncta (normalized for the cytosolic Sec24C) at the indicated cell confluency. Mean  $\pm$  s.e.m. of a representative experiment out of five biological replicates.  $n = 50$ –80. ns: not significant; \*\*\*\* $P < 0.0001$ , one-way ANOVA with Dunnett's multiple comparison test.
- D Differentiation of podocytes. Western blot of growing and differentiated podocytes. Synaptopodin (SYNPO) was used as a differentiation marker, GAPDH as a loading control.
- E Growing and differentiated podocytes were treated with SA (300  $\mu$ M, 30 min) and stained for TRAPPC2 or Sec24C and eIF3. Scale bar, 10  $\mu$ m. The graphs show quantification of TRAPPC2 and Sec24C (mean intensity) in SGs. Mean  $\pm$  s.e.m. of three independent experiments. \*\*\*\* $P < 0.0001$ , Student's unpaired two-tailed  $t$ -test.
- F Western blot analysis of total (RB) and phosphorylated (p-RB) retinoblastoma in growing (non-differentiated) versus differentiated podocytes.  $\beta$ -Actin was used as loading control.
- G CDK kinase activity in growing and differentiated podocytes. Western blot using a specific antibody recognizing phosphoSer-CDK substrates was used on total cell lysates.

Source data are available online for this figure.

morphology of the GC in cells exposed to oxidative stress under conditions that prevent COPII/TRAPP recruitment to SGs (i.e., treatment with CDK inhibitors, and highly confluent cells) or that impair SG formation (i.e., treatment with ISRIB). We found that CDK inhibitors prevented the fragmentation of the GC in cells exposed to oxidative stress (Fig 9B) and that oxidative stress had no impact on the organization of the Golgi complex in highly confluent cells (Fig 9C). Finally, ISRIB was effective in preventing the fragmentation of the Golgi complex induced by SA (Fig 9D).

These results are consistent with the hypothesis that TRAPP/COPII sequestration on SGs can induce Golgi fragmentation. To gain insights into the nature of the fragmentation of the Golgi complex, we performed ultrastructural analysis that revealed the presence of residual swollen cisternae with the loss of stacked structures and extensive vesiculation in SA-treated cells (Fig 9E), a situation that is reminiscent

of the effect of Rab1 inactivation (Wilson *et al*, 1994). We hypothesized that the dismantling of the Golgi complex could have been due to impaired Rab1 activation as a consequence of TRAPP (the Rab1 GEF) sequestering to SGs. We monitored Rab1 activity by using an antibody that specifically recognizes the GTP-bound Rab1 and found, indeed, that the fraction of active Rab1 (i.e., the GTP-bound form) is progressively reduced in cells exposed to SA (Fig 9F). Of note, increasing Rab1 levels by overexpression reduced fragmentation/vesiculation of the GC induced by oxidative stress without affecting the capacity of TRAPP to migrate to SGs (Figs 9G and EV5D).

It is worth mentioning that a further contribution to the disorganization of the Golgi complex upon oxidative stress may derive from the delocalization of the TGN-located PARP12 to SGs, which, however, affects mainly late Golgi compartments (Catara *et al*, 2017).

**Figure 7. The TRAPP complex controls SG composition and function.**

- A SG area (see Materials and Methods) in mock, TRAPPC2, TRAPPC3, TRAPPC8, and TRAPPC9-depleted cells treated with SA. Data are shown in box-and-whisker plots: box-plot central line, median; box limits, upper and lower quartiles; whiskers show the minimum to maximum.  $N = 3$ . \*\*\*\* $P < 0.001$ , \*\*\*\* $P < 0.0001$ , one-way ANOVA with Dunnett's multiple comparison test.
- B HeLa cells microinjected with control IgG or a TRAPPC3-specific antibody (right panels in green) were treated with SA. The TRAPPC3 Ab disrupts the Golgi (Yu *et al*, 2006), monitored using an anti-TGN46 Ab. Anti-G3BP was used to stain SGs. The graph shows quantification of the SG area. Mean  $\pm$  s.e.m. three independent experiments;  $n > 80$ . \*\*\*\* $P < 0.0001$ , Student's unpaired two-tailed  $t$ -test. Scale bar, 10  $\mu$ m.
- C Structured illumination microscopy (SIM)-super resolution (SR) images of endogenous TRAPPC2 and GFP-Sec23 localizing at SGs, stained for G3BP. Scale bar, 5  $\mu$ m. Right, magnification of boxed area. Scale bar, 0.5  $\mu$ m.
- D, E Localization of Raptor (D) and RACK1 (E) in mock, TRAPPC3-KD, and TRAPPC2-KD HeLa cells treated with SA. G3BP was used to stain SGs. Scale bar, 10  $\mu$ m. Each graph shows the quantification (mean intensity) of the respective protein in SG spots expressed as a percentage of the mock (TRL). Mean  $\pm$  s.d. three independent replicates. \* $P < 0.02$ ; \*\* $P < 0.009$  in (D), \* $P < 0.05$ ; \*\*\*\* $P < 0.0001$  in (E), one-way ANOVA with Dunnett's multiple comparison test.
- F, G Immunoprecipitation (IP) with an anti-TRAPPC2 Ab or IgG from cells with or without SA treatment, as indicated, followed by SDS-PAGE and Western blot with anti-Raptor (F) or anti-RACK1 (G) Abs. Input: cell lysate (40  $\mu$ g for TRAPPC2, 10  $\mu$ g for RACK1 and Raptor).
- H, I Localization of Raptor (H) and RACK1 (I) in untreated cells or cells pre-treated with the indicated CDK inhibitor (1  $\mu$ M, 150 min) and then with SA (300  $\mu$ M, 30 min). G3BP was used to stain SGs. Scale bar, 10  $\mu$ m. Graphs show quantification of the localization of the respective protein with SGs, expressed as a percentage of the control. Mean  $\pm$  s.e.m. of one representative experiment out of three independent replicates,  $n = 60$ –80. \*\*\*\* $P < 0.0001$ , one-way ANOVA with Dunnett's multiple comparison test.
- J Analysis of cell death after overnight recovery of HeLa cells treated or untreated with CDKi (SNS-032; flavopiridol or dinaciclib, 1  $\mu$ M, 150 min) and then treated or not with SA (500  $\mu$ M, 3 h). Images were acquired automatically by OPERETTA microscope. Values indicate the percentage of the total number of nuclei (stained with DAPI) positive for BoBo-3 staining. Mean  $\pm$  s.d. of one representative experiment out of three independent replicates. ns: not significant, \*\*\*\* $P < 0.0001$ , one-way ANOVA with Dunnett's multiple comparison test.
- K Analysis of cell death, as described in (J), in HeLa cells that were left untreated, treated with non-targeting siRNAs or siRNAs against TRAPPC2, and in two cell clones knocked out for TRAPPC2, with and without SA treatment. Mean  $\pm$  s.d. of three independent replicates.

Source data are available online for this figure.

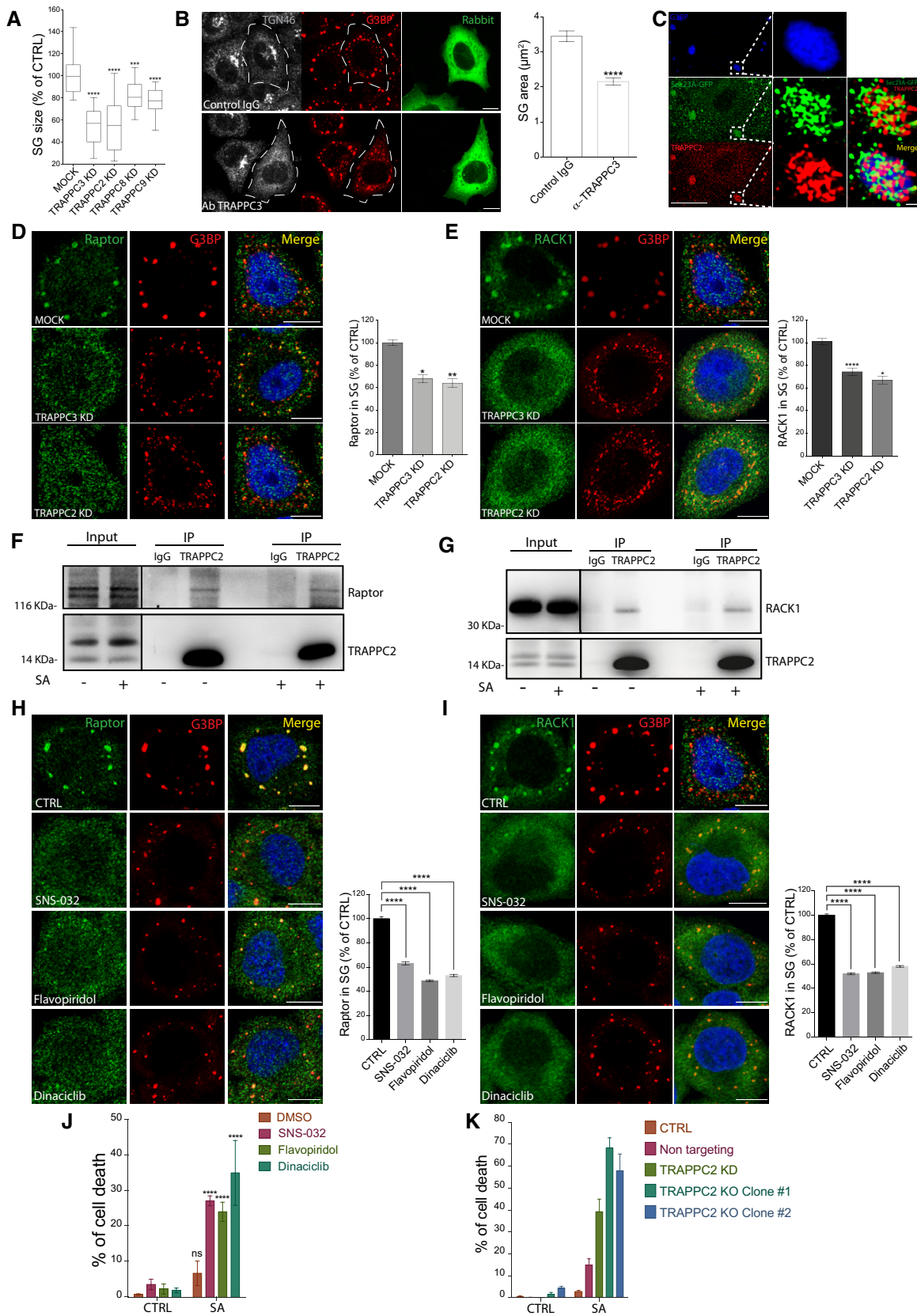


Figure 7.



**Figure 8. The sequestering of TRAPP and COPII in SGs slows down ER export.**

- A Left, control or SA-treated (500  $\mu$ M, 120 min) human fibroblasts (HFs) were incubated at 40°C for 180 min and stained for eIF3, PCI, and Sec24C. Right, the cells were imaged 10 min after shifting the temperature from 40°C to 32°C and stained for eIF3, PCI, and Giantin (to label the Golgi).
- B HeLa cells were exposed to SA (200  $\mu$ M) for the indicated time, alone or in combination with ISRIB and SGs were analyzed. Quantification of SG area ( $\mu$ m) of three independent experiments. Mean  $\pm$  s.e.m.  $n$  = 60–80 cells per experiment,  $N$  = 3.
- C Quantification of Sec24C localization at SGs over time (the ratio between Sec24C (mean fluorescence intensity) in SG puncta and cytosolic Sec24C). Mean  $\pm$  s.d.  $n$  = 60–80 cells per experiment,  $N$  = 3.
- D HeLa cells expressing VSV-G-UVR8 mEOS were left untreated or treated with SA alone or in combination with ISRIB (1  $\mu$ M; 120 min ISRIB pre-treatment and 30 min SA+ISRIB) and then pulsed with blue light. Images were taken 10 min after the UV pulse and processed for staining with the indicated markers.
- E Cells were treated with SA for 30 min, the SA was washed out (WO), and cells were left to recover for 120 min in the presence of cycloheximide, followed by a blue light pulse and processing for staining as described in (D).
- F Quantification of VSV-G (mean intensity) in the Golgi area to the total VSV-G per cell under the conditions described in (D, E). Data are expressed as percentage of the control. Mean  $\pm$  s.e.m. of three independent experiment. \*\*\*\* $P$  < 0.0001; ns: not significant, one-way ANOVA with Dunnett's multiple comparison test.
- Data information: (A, D, E) Scale bars, 10  $\mu$ m.

## Discussion

We described a branch of the integrated stress response that is dependent on the assembly of SGs and that impinges on the early secretory pathway. A key player of this branch is TRAPP, a multi-molecular complex that intervenes in multiple membrane trafficking steps.

We showed that TRAPP is massively recruited to SGs in response to different acute stress stimuli and in turn recruits Sec23-Sec24 (components of the inner layer of the COPII complex, the protein complex that drives the export of newly synthesized proteins from the ER) to SGs. The functional consequences of the recruitment of TRAPP/COPII to SGs are double-edged since on the one hand they impact on the function and organization of the secretory pathway while on the other they impact on the composition and function of the SGs.

We have shown that the sequestering to SGs of these two complexes, one (COPII) with a pivotal role in ER export and another (TRAPP) acting as a GEF for Rab1, a master GTPase orchestrating the organization of the Golgi complex, induces a slow-down of the ER-to-Golgi transport of newly synthesized proteins and the disorganization of the structure of the Golgi complex. This halt in secretory activity, an energetically costly process, can be seen as a way to limit energy expenditure upon acute stress but also to prevent the ER export of newly synthesized proteins that might have been damaged/misfolded by the acute stress before an adequate UPR is

installed and becomes operative. Importantly, these changes are completely reversible since ER export resumes and proper Golgi morphology is restored upon stress removal and relocation of the two complexes to their natural sites.

An intriguing feature of this branch of the integrated stress response that involves the secretory pathway is its strict dependence on the proliferation status of the cells. Indeed, the sequestration of TRAPP and COPII to SGs occurs only when the acute stress affects actively proliferating cells. Cells with a slow/halted proliferation rate still form SGs in response to acute stress stimuli, but do not delocalize TRAPP/COPII from their steady-state sites, i.e., the ERES, to SGs. We have used multiple strategies to slow down (or halt) proliferation: nutrient deprivation, a high cell density, or a switch from a proliferation to a differentiation program. Under all circumstances, we observed a very tight correlation between the extent of recruitment of TRAPP/COPII to SGs and the proliferation rate, indicating that acquisition of components of the secretory machinery does not occur by default as a consequence of the assembly of the SGs but is an active process that is subject to specific regulation.

We found that this regulation involves the activity of CDK1/2. CDK1/2 inhibitors and/or CDK1/2 downregulation prevent the relocation of TRAPP/COPII to SGs by a dual mechanism: They hamper their association with SGs mediated by the CDK substrate hnRNPk and they reduce their mobilization from ERES.

The function of the ERES and COPII coat is known to be under CDK control. A member of the CDK family, PCTAIRE, is recruited to

**Figure 9. The sequestering of TRAPP in SGs induces the fragmentation of the GC in a Rab1-dependent manner.**

- A AiryScan images of HeLa cells treated with SA for the indicated times and stained with GM130 (gray). Scale bar, 10  $\mu$ m. The graph shows quantification of Golgi objects in SA-treated cells. Mean  $\pm$  s.e.m. of three independent experiments.  $n$  = 90–100. \*\*\*\* $P$  < 0.0001; ns: not significant, Student's unpaired two-tailed  $t$ -test.
- B Control cells and cells treated with dinaciclib (CDKi) were treated with SA and stained for GM130 (in gray). Insets, eIF3. Blue, nuclear DAPI staining. The graph shows quantification of Golgi objects in HeLa cells untreated or treated with SNS-032, flavopiridol, or dinaciclib for 150 min and then treated with SA (300  $\mu$ M, 30 min). Mean  $\pm$  s.e.m. of three independent experiments. \*\*\*\* $P$  < 0.0001, one-way ANOVA with Dunnett's multiple comparison test.
- C Quantification of Golgi objects in cells plated at different percentage of confluency and treated or untreated with SA. Mean  $\pm$  s.e.m. of three independent experiments. \*\* $P$  < 0.001; \*\*\* $P$  < 0.0002; ns: not significant, one-way ANOVA with Dunnett's multiple comparison test.
- D Quantification of Golgi objects in cells pre-treated with ISRIB (1  $\mu$ M) for 3 h and then exposed to SA (30 min) in the presence of ISRIB. \*\*\* $P$  < 0.002, Student's unpaired two-tailed  $t$ -test.
- E Electron microscopy images of cells treated (300  $\mu$ M, 30 min) or untreated with SA. The arrow indicates the Golgi complex. Scale bar, 200 nm.
- F AiryScan images of HeLa cells at steady state or exposed to SA for the indicated times. A Rab1-GTP-specific antibody was used to monitor the pool of active Rab1, and GM130 to stain the Golgi complex. Insets, eIF3. Scale bar, 10  $\mu$ m. The graph shows quantification of Rab1-GTP at the Golgi complex expressed as a percentage of the control. Mean  $\pm$  s.e.m. of three independent experiments. \* $P$  < 0.011, \*\* $P$  < 0.002, Student's unpaired two-tailed  $t$ -test.
- G HeLa cells transfected or not with WT GFP-Rab1B were left untreated or treated with SA and stained for GM130 and G3BP to monitor SGs. Dashed white line, WT GFP-Rab1B transfected cells. Scale bar, 10  $\mu$ m. The graph shows quantification of Golgi objects in the different conditions. NT: non-transfected. Mean  $\pm$  s.e.m. of three independent experiments. \*\*\*\* $P$  < 0.0001, Student's unpaired two-tailed  $t$ -test.

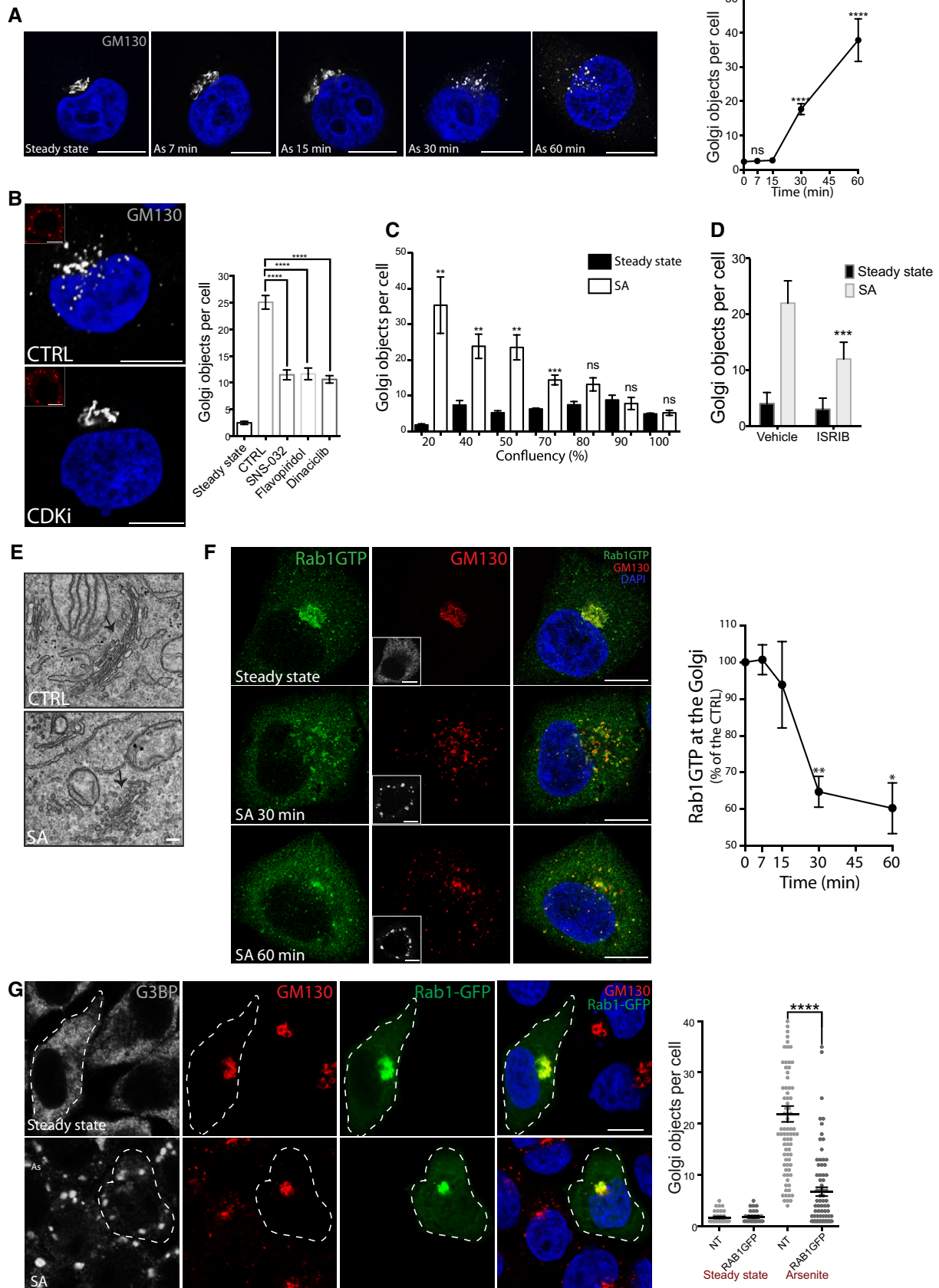


Figure 9.

ERES via its interaction with Sec23 and controls ER export (Palmer *et al*, 2005), while Sec31, a component and a regulator of Sar1/COPII cycle, can be phosphorylated by CDKs (Holt *et al*, 2009; Hu *et al*, 2016). Further, the phosphorylation of Sec31 in response to growth factor and mitogenic signals has also been reported (Olsen *et al*, 2006; Dephoure *et al*, 2008). We have shown here that, consistent with the described role of Sec31 as a co-GAP for Sar1, Sec31 function is required to control the COPII cycle at the ERES, since Sec31 depletion induces a tighter association of Sec23-24 with ERES and prevents their translocation to SGs. In fact, our results indicate that the extent of translocation of COPII/TRAPP to SGs is directly proportional to their cycling rate at the ERES membranes. We have shown that this rate is diminished not only by CDK inhibitors but also, importantly, in starved cells compared to actively proliferating cells. These observations are in line with previous reports showing that the cycling rate of ERES components is under control of growth factors and growth factor-dependent signaling (Farhan *et al*, 2010; Tillmann *et al*, 2015). Thus, the activity of the ERES, as measured by their number and by the rate of cycling of COPII and other ERES components, is stimulated under conditions that demand maximal output efficiency from the ER (i.e., during cell proliferation) as they involve cell size increase and organelle expansion. If cells experience an acute stress under these conditions of active growth, then the fast cycling COPII components are susceptible to being temporarily sequestered to the SGs to instantly slow down ER output and reduce energy consumption. By contrast, conditions that are not permissive for cell proliferation, such as nutrient starvation, stabilize the association of COPII/TRAPP with ERES membranes and prevent their translocation to SGs. Indeed, a profound remodeling of ERES is known to occur during nutrient starvation and coincides with the rerouting of COPII and TRAPP from their role in mediating the ER export of newly synthesized proteins to their role in autophagosome formation (Imai *et al*, 2016; Kim *et al*, 2016; Lamb *et al*, 2016; Ge *et al*, 2017; Ramírez-Peinado *et al*, 2017; van Leeuwen *et al*, 2018). The kinetics of the COPII cycling at the sites of phagosome formation in the ER have not been specifically explored. It is tempting to speculate that it might be slower than that at the “conventional” ERES under feeding conditions and that this more stable association of COPII with the ER during autophagosome formation may in turn prevent its sequestration to SGs upon stress exposure. Preventing the sequestration of TRAPP/COPII in starved cells exposed to stress would preserve the function of COPII and TRAPP in the autophagy process, a process that leads to nutrient recycling and energy production, two desirable events in cells exposed to stress.

Finally, we have shown that TRAPP is required for the proper maturation of SGs. Impeding the recruitment of TRAPP to SGs or depleting TRAPP does not impair the formation of SGs *per se* but hampers their maturation, as evaluated by their size (smaller SGs in the absence of TRAPP) and composition. We found that two key signaling components, RACK1 and Raptor, which are normally recruited to SGs, are TRAPP interactors and that they are no longer recruited to SGs in TRAPP-depleted cells. This impaired recruitment of RACK1 and Raptor to SGs renders TRAPP-depleted cells less resistant to stress and more prone to undergo apoptosis, as the association of these signaling elements with SGs exerts an anti-apoptotic role (Arimoto *et al*, 2008; Thedieck *et al*, 2013; Wippich *et al*, 2013).

Our finding that TRAPP, and in particular TRAPPC2, acts as a mediator of the secretory arrest in response to stress and as a driver of SG maturation elicits the question as to whether and how these unsuspected properties of TRAPPC2 may be relevant for the pathogenesis of SEDT, which is caused by mutations in TRAPPC2 (Gedeon *et al*, 1999). These, as well as the more general question concerning the physiological relevance of assembling SGs in response to stress (Protter & Parker, 2016), remain outstanding questions for further investigation. For now, we can only speculatively propose that, given the role of TRAPPC2 in mediating secretory arrest and SG maturation in actively proliferating cells, the main target cells in SEDT are likely to be proliferative chondrocytes. Derived from chondrocyte progenitor cells, rapidly proliferating chondrocytes are key components of the epiphyseal growth plate and undergo terminal differentiation into postmitotic hypertrophic chondrocytes, which eventually transdifferentiate into osteoblasts or undergo apoptosis, being replaced by osteoblasts and osteoclasts. It is established that the rate of proliferation, together with the height of columnar hypertrophic chondrocytes, is major determinant of growth plate function and thus of bone length (Ballock & O’Keefe, 2003). We hypothesize that TRAPPC2-defective proliferative chondrocytes are less resistant to repetitive stresses, including mechanical and oxidative stresses (Henrotin *et al*, 2003; Zuscik *et al*, 2008), and are thus more prone to undergo apoptosis. The accelerated loss of proliferative chondrocytes would thus lead to a premature growth plate senescence that could manifest as progressive delayed growth.

## Materials and Methods

### Reagents and antibodies

Primary antibodies used in this study were mouse monoclonal antibody anti-G3BP (BD Transduction Laboratories cat. no. 611126), rabbit polyclonal antibody anti-G3BP (Bethil, cat. no. A302-033), mouse monoclonal antibody anti-TRAPPC5 (Abnova cat. no. H00126003-A01), rabbit polyclonal antibody TRAPPC8 (Sigma-Aldrich cat. no. HPA041107), mouse monoclonal antibody TRAPPC9 (Proteintech cat. no. 16014-1-AP), goat polyclonal antibody anti-eIF3 (Santa Cruz cat. no. sc-16377), rabbit polyclonal antibody anti-Sec24C (Sigma-Aldrich cat. no. HPA040196), rabbit monoclonal antibody anti-Sec24B (Cell Signaling cat. no. 12042S), rabbit polyclonal antibody anti-Sec24A (Cell Signaling cat. no. 9678), mouse monoclonal antibody anti-Sec24D (Santa Cruz, cat. no. sc-101268), mouse monoclonal anti-TIAR (BD Transduction Laboratories cat. no. 610352), mouse monoclonal TRAPPC12 (Abcam cat. no. 88751), mouse monoclonal TRAPPC10 (Santa Cruz cat. no. SC-101259), mouse monoclonal anti-Flag (Sigma-Aldrich cat. no. F1804), rabbit polyclonal antibody anti-phosphor-Ser CDK substrates motif (Cell signaling cat. no. 9477), mouse monoclonal anti-GM130 (BD Transduction Laboratories cat. no. 610823), human monoclonal antibody anti-Rab1-GTP (Adipogen cat. no. AG-27B-0006), mouse monoclonal anti-RACK1 (Santa Cruz cat. no. 17754), rabbit polyclonal anti-Raptor (Cell signaling cat. no. 2280), rabbit polyclonal Sec16A (Bethil, cat. no. A300-648A), sheep polyclonal anti-TGN46 (Serotec cat. no. AHP500), rabbit polyclonal antibody anti-Sec31A (Sigma-Aldrich cat. no. HPA005457), mouse monoclonal antibody AP-II (Pierce, cat. no. MA1-064), mouse monoclonal  $\gamma$ -adaptin (Transduction cat. no. 618305), mouse monoclonal

antibody anti-retinoblastoma (Cell Signaling cat. no. 9309), rabbit polyclonal antibody anti-phospho retinoblastoma (Cell Signaling cat. no. 9516), rabbit polyclonal antibody anti-eIF2 $\alpha$  (Cell Signaling cat. no. 9722), rabbit polyclonal antibody anti-phospho-eIF2 $\alpha$  (ser51) (Cell Signaling cat. no. 3597), mouse monoclonal antibody anti-puromycin (Millipore cat.no. MABE343), rabbit polyclonal anti- $\beta$ -actin (Sigma-Aldrich cat. no. A2066), mouse monoclonal antibody anti-GAPDH (Santa Cruz cat. no. sc-32233). Guinea pig polyclonal antibody anti-Synaptopodin (Acris cat. no. AP33487SU-N). Rabbit monoclonal antibody anti-hnRNPk (Abcam #ab52600). Polyclonal antibodies against Arfaptin, p115, G-97, COPI, TRAPPC2, and TRAPPC3 were obtained in our laboratories. Media, serum, and reagents for tissue culture were purchased from Thermo Fisher Scientific.

Sodium arsenite (cat. no. S7400), puromycin (cat.no. A1113802), and cycloheximide (cat.no. C7698) were purchased from Sigma-Aldrich; flavopiridol hydrochloride (cat. no. S2679), SNS-032 (BMS-387032) (cat. no. S1145) and dinaciclib (SCH727965) (cat. no. S2768) were purchased from Selleckchem. DSP (dithiobis(succinimidyl propionate) Lomant's reagent was purchased from Thermo Fisher Scientific (Catalog no. 22585).

### Plasmid construction

TRAPPC3-GFP, Sec23A-GFP, Sar1GTP-GFP, Rab1-GFP, OCRL-GFP, Rab5-GFP, and Rab7-GFP were obtained as previously described (Vicinanza *et al*, 2011; Venditti *et al*, 2012; De Leo *et al*, 2016). The construct encoding GFP-ARF1 has been described (Dubois *et al*, 2005). NHA-hnRNPk was a gift from Igor Ulitsky (Addgene plasmid #120389). The previously described TRAPPC2 constructs (WT, D47Y, R90X; Venditti *et al*, 2012) were recloned into the p3XFLAG-CMV<sup>TM</sup>-10 Expression Vector (Sigma, E7658).

### Cell culture, transfection, and RNA interference

HeLa cells were grown in high glucose (4,500 mg/l) DMEM supplemented with 10% FCS. U2OS was grown in McCoy's supplemented with 20% FCS. Human fibroblasts were grown in DMEM and M199 (1:4) supplemented with 10% FCS. Podocytes were grown in RPMI-1640 supplemented with 10% insulin–transferrin–selenium (ITS) and 10% FCS.

For transfection of DNA plasmids, HeLa cells were transfected using either TransIT-LT1 (Mirus Bio LLC, for BioID2 experiment) or JetPEI (Polyplus, for immunofluorescence analysis) as transfection reagents, and the expression was maintained for 16 h before processing. Microinjection of TRAPPC3 antibody was performed as described (Venditti *et al*, 2012).

siRNA sequences used in this study are listed in Appendix Table S1. HeLa cells were treated for 72 h with oligofectamine (Life Technologies) for direct transfection.

Knock-down efficiency was evaluated by Western blot for the indicated TRAPP components and Sec31 (Appendix Fig S1) and by qRT-PCR for CLIC1, CRYAB, ENO1, Sec23 and Sec24 isoforms, Sec16, CDK1, CDK2 (Fig EV3 and Appendix Fig S1).

### Generation of TRAPPC2 KO cell line

SEDL-KO HeLa cells were generated by double infection with lentiviral particles (LentiArray Particles, Thermo Fischer Scientific), one

lentiviral containing a cassette for expression of a gRNA sequence (GTTCAACGAGTGGTTTGTGT) to target TRAPPC2 and the other to express Cas9. The cells were co-infected at 70% confluency with a MOI of 1:10 gRNA:CAS9 in the presence of 5  $\mu$ g/ml of polybrene (Sigma). After 48 h, the cells were incubated in medium containing 1  $\mu$ g/ml of puromycin (Calbiochem) and 0.5  $\mu$ g/ml blasticidin (Invivogen). After a further 5 days, single-cell sorting in 96-well plates was performed using FACSARIA III from Becton Dickinson (BD Biosciences, San Jose, USA). Two to three weeks later, single clones were detached and analyzed by PCR and subsequent sequencing. Positive clones were further verified by SDS–PAGE and immunofluorescence analysis.

### Stress stimuli

Mammalian cells were treated with 300  $\mu$ M SA for 30 min (unless otherwise stated) in DMEM 10% FBS supplemented with 20 mM Hepes. Temperature was maintained at 37°C for the time of treatment in a water bath. Heat treatment (44°C) was for 45 min in a water bath.

### Immunofluorescence microscopy

HeLa, human fibroblasts, U2OS, and rat chondrosarcoma cells were grown on coverslips and fixed with 4% PFA for 10 min, washed three times with PBS, blocked, and permeabilized for 5 min in 0.1% Triton in PBS. Samples were washed three times and blocked with blocking solution (0.05% saponin, 0.5% BSA, 50 mM NH<sub>4</sub>Cl in PBS) and incubated with primary antibodies diluted in blocking solution for 1 h at RT. Coverslips were washed with PBS and incubated with fluorochrome-conjugated secondary antibodies (Alexa-Fluor-488, Alexa-Fluor-568 and Alexa-Fluor-633) for 1 h at RT. Fixed cells were mounted in Mowiol and imaged with Plan-Apochromat 63 $\times$ /1.4 oil objective on a Zeiss LSM800 confocal system equipped with an ESID detector and controlled by a Zen blue software. Fluorescence images presented are representative of cells imaged in at least three independent experiments and were processed with Fiji (ImageJ; National Institutes of Health) software. Quantification of the amount of TRAPPC2 or Sec24C at ERES was calculated by co-staining cells for ERES markers, such as Sec31 or cTAGE5, and normalizing to the total amount of TRAPPC2 or Sec24C. The amount of TRAPP components or Sec24C in SGs was calculated as the ratio between TRAPP components or Sec24C (mean fluorescence intensity) in SG puncta and cytosolic TRAPP components or Sec24C. Differences among groups were performed using the unpaired Student's *t*-test calculated with the GraphPad Prism software. All data are reported as mean  $\pm$  s.e.m. as indicated in the figure legends.

For Structured Illumination Microscopy (SIM, Fig EV4), cells were imaged with a Plan-Apochromat 63 $\times$ /1.4 oil objective on a Zeiss LSM880 confocal system. Image stacks of 0.88  $\mu$ m thickness were acquired with 0.126  $\mu$ m z-steps and 15 images (three angles and five phases per angle) per z-section. The field of view (FOV) was  $\sim$ 75  $\times$  75  $\mu$ m at 0.065  $\mu$ m/pixel, and a SIM grating of 34  $\mu$ m was used. Image stacks were processed and reconstructed with Zen software, using the SIM tool in the Processing palette.

## Gel filtration

The lysate used for gel filtration was prepared by cell cracker homogenizing  $1.8 \times 10^8$  cells in 2 ml of buffer 20 mM HEPES, pH 7.2, 150 mM NaCl, 2 mM EDTA, 1 mM DTT, and Protease inhibitor (Roche). The sample was centrifuged at  $100,000 \times g$  for 1 h. Ten milligrams of protein was concentrated to 350  $\mu$ l and loaded onto a Superose6 gel filtration column (GE), and 400  $\mu$ l fractions were collected. Fifty microliters of each fraction was processed for SDS-PAGE analysis, and proteins were detected by Western blot using specific antibodies as described in Fig EV1F.

## Yeast methods

The centromeric plasmid pUG23-Bet3-GFP (His selection) was described previously (Mahfouz *et al*, 2012). A Pab1-mRFP expressing plasmid was constructed by PCR amplification of the Pab1 gene plus 419 bp of the promoter region from yeast genomic DNA and cloning into the vector backbone of the centromeric plasmid pUG35 (Ura selection), removing the Met25 promoter and replacing GFP with mRFP, using standard cloning techniques. Yeast cells (BY4743) were transformed with both plasmids and grown in—Ura-His media with 2% dextrose at 30°C to early log phase. Stress granules were induced by incubating cells at 46°C for 10 min (Riback *et al*, 2017) and observed immediately on an LSM800 microscope.

## Immunoprecipitation

HeLa cells were transfected with the TRAPPC2-3XFLAG and 3XFLAG constructs. Sixteen hours post-transfection, cells were left untreated or treated with SA (300  $\mu$ M, 30 min). Following lysis (50 mM Tris-HCl pH 7.4, 100 mM NaCl, 1 mM EDTA, 0.5% lauryl maltoside, protease and phosphatase inhibitors), cell extracts (5 mg/sample) were immunoprecipitated for 5 h at 4°C using M2 anti-FLAG Ab. Immunoprecipitates were analyzed by LC-MS/MS (see below).

Co-immunoprecipitation of Raptor (Fig 7F), RACK1 (Fig 7G), and endogenous hnRNPK (Fig 5E) with TRAPP complex using the anti-TRAPPC2 Ab was performed on cell extracts after cross-linking. Cross-linking was performed on HeLa cells by washing 3 times with PBS 1 $\times$ , incubating for 30 min with 1 mg/ml DSP in PBS 1 $\times$ , 0.8% DMSO at RT. The reactions were stopped by adding Tris pH 8.0 to a final concentration of 100 mM for 10 min. The cells were washed three times in PBS 1 $\times$  and lysed in 20 mM HEPES pH 7.3, 1 mM EDTA, 0.5% deoxycholate, 0.5% NP-40, 0.05% SDS plus protease inhibitors. After 10 passages in a 26-gauge syringe needle and six cycles of freeze and thaw, particles were removed at  $20,000 \times g$  for 10 min at 4°C. Cell lysates (2 mg/sample) were then IP with anti-TRAPPC2 Ab or with control IgG and the immunoprecipitated proteins were analyzed by SDS-PAGE and Western blot with the indicated Ab.

## LC-MS/MS

Immunoprecipitated proteins were eluted and reduced in Laemmli buffer with 10 mM TCEP, boiled, and alkylated with 120 mM acrylamide and fractionated by SDS-PAGE. Gel lanes were cut into three pieces and digested as previously described (Shevchenko *et al*, 2006). In brief, gel pieces were washed, destained, dehydrated, and digested subsequently (1:100 ratio) overnight at 37°C with

sequencing grade trypsin (Promega; Madison, WI, USA). The resulting peptides were extracted using increasing acetonitrile concentrations. The peptide mixtures were concentrated and desalted using the Stop and Go Extraction (STAGE) technique (Rappsilber *et al*, 2003). Samples for LC-MS/MS analysis were loaded on a NanoLC 1200 coupled via a nano-electrospray ionization source to a quadrupole-based Q Exactive HF benchtop mass spectrometer (Michalski *et al*, 2011). Peptide separation was carried out according to hydrophobicity on a 250 mm PicoFrit column (New Objective, Inc., cat. PF7508-250H363) using a binary buffer system consisting of solution A: 0.1% formic acid and B: 80% acetonitrile, 0.1% formic acid. Runs of 75 min were used for immunoprecipitated samples. Linear gradients from 7 to 32% B were applied with a following increase to 95% B at 300 nl/min. Q Exactive HF settings: MS spectra were acquired using 3E6 as an AGC target, a maximal injection time of 20 ms and a 120,000 resolution at 200 m/z. The mass spectrometer operated in a data-dependent Top15 mode with subsequent acquisition of higher energy collisional dissociation (HCD) fragmentation MS/MS spectra of the top 15 most intense peaks. Resolution for MS/MS spectra was set to 45,000 at 200 m/z, AGC target to 1E5, max injection time to 85 ms and the isolation window to 1.4 Th. The intensity threshold was set at 2.0E4 and Dynamic exclusion at 20 s.

In total, we identified 1,992 proteins. The proteins that had probability values ( $P$ ) < 0.05 and ratio > 1.5 (log difference > 0.6) in the IP of TRAPPC2-FLAG-transfected cells compared to the FLAG-transfected cells were considered statistically significant. Two hundred and forty-one proteins were specifically IP with TRAPPC2 under steady-state conditions, and 335 proteins were specifically IP with TRAPPC2 under SA treatment. Out of the 241 proteins co-IP with TRAPPC2 under steady-state conditions, 49 are known SG components with 20 of them being RBPs; out of the 335 proteins co-IP with TRAPPC2 under SA treatment, 82 are known SG components, with 53 of them being RBPs (Jain *et al*, 2016; Markmiller *et al*, 2018; Youn *et al*, 2018).

Fifty-three RBPs (determined from GOMF terms in Perseus) were co-IP with TRAPPC2 under steady-state conditions and 87 were co-IP with TRAPPC2 upon SA treatment.

## Digitonin assay

HeLa cells were exposed to SA or treated with dinaciclib (10  $\mu$ M). After treatment, cells were washed twice with permeabilization buffer (25 mM HEPES, 125 mM CH<sub>3</sub>COOK, 2.5 mM Mg(CH<sub>3</sub>COO)<sub>2</sub>, 5 mM EGTA, 1 mM DTT) and then permeabilized in PB buffer supplemented with 30  $\mu$ g/ml of digitonin plus the indicated antibody to visualize permeabilized cells. To analyze Sec24C association with SGs, digitonin was left for 6 min at room temperature. Cells were then washed three times with PB buffer and left in PB buffer for 10 min at RT. Finally, samples were fixed with 4% PFA and processed for IF. To analyze Sec24C association at ERES in the presence of dinaciclib, cells were fixed for 2 min after digitonin permeabilization.

## High-content screening

HeLa cells were plated in 384-well culture plates. The day after, a kinase inhibitor library, purchased from Selleckchem, was dispensed using a liquid-handler system (Hamilton) to give a final concentration of 10  $\mu$ M. One hundred and fifty minutes after drug

administration, cells were treated with sodium arsenite (300  $\mu$ M) for 30 min at 37°C in the presence of compounds. Finally, samples were fixed for 10 min at room temperature by adding 1 volume of 4% PFA (paraformaldehyde in PBS) to the growth medium and stained with the appropriate antibodies.

For image acquisition, at least 20 fields were acquired per well (average 1,000 cells/well) of the 384-well plate using confocal automated microscopy (Opera high-content system; Perkin-Elmer). A dedicated script was developed to perform the analysis of Sec24C localization on the different images (Harmony and Acapella software; Perkin-Elmer). The script calculated the co-localization value of Sec24C with the SG marker (G3BP). The results were normalized using positive (mock cells exposed to SA) control samples in the same plate.

*P*-values were calculated on the basis of mean values from three independent wells. The data are represented as a percentage of Sec24C recruitment in the control cells (100%) using Excel (Microsoft) and Prism software (GraphPad software).

### Cell cycle analysis by flow cytometry

HeLa cells were harvested and resuspended in PBS. For the fixation, a ninefold volume of 70% ethanol was added and incubated at 4°C for at least 1 h. Next, cells were centrifuged, washed in PBS, and resuspended in PBS containing RNase A 0.1 mg/ml. After incubation for 1 h at 37°C, propidium iodide was added to a final concentration of 10  $\mu$ g/ml and samples were analyzed in an Accuri C6 flow cytometer.

### Cell proliferation analysis by high-content imaging

Cell cycle analysis by high-content imaging was performed using the Click-iT Plus EdU Alexa-Fluor 488 Imaging Kit (Life Technologies) according to the manufacturer's instructions. Images were acquired with an automated confocal microscopy (Opera System, Perkin-Elmer) and analyzed through Columbus Image Data Storage and Analysis System (Perkin-Elmer). Nuclear intensity of EdU (5-ethynyl-2'-deoxyuridine, a nucleoside analog of thymidine) in EdU-positive nuclei (S-phase cells) was used as a measure of DNA replication rate.

### Cell death assay

HeLa cells were pre-treated with CDK inhibitors (SNS-032, flavopiridol, and dinaciclib) for 150 min and exposed to SA (500  $\mu$ M, 1 h). Subsequently, the stress stimulus was washed out and cells left to recover for 16 h. To stain dead cells, a fluorophore dye cocktail containing the cell-permanent nuclear dye Hoechst 33342 and the cell-impermeant nuclear dye BOBO<sup>TM</sup>-3 that selectively labels dying cells (Invitrogen, H3570, B3586), was added to the growth media and incubated for 45 min (37°C, 5% CO<sub>2</sub>). Cells were analyzed by automated microscopy (Operetta high-content system; Perkin-Elmer) using a customized script to calculate the ratio between BOBO<sup>TM</sup>-3 positive nuclei and total cells.

### Puromycin assay

The puromycin (PMY) assay was modified from David *et al* (2012). In brief, mock, TRAPPC2-KD or TRAPPC3-KD HeLa cells were exposed to SA (500  $\mu$ M, 30 min) in DMEM 10% FCS. Cells were washed three times in DMEM 1 $\times$  and incubated with 9  $\mu$ M PMY in

DMEM for 5 min at 37°C. Samples were lysed in RIPA buffer and processed for Western blot analysis with the anti-puromycin antibody.

### Transport assays

VSVG-mEOS2-2XUVR8 was a gift from Matthew Kennedy (AddGene plasmid #49803). HeLa cells were transfected with the plasmid for 16 h and treated with SA, CHX, and ISRIB for the indicated times. A UV-A lamp was used to illuminate samples (4 pulses, 15 s each). After the light pulses, cells were left for 10 min at 37°C, then fixed with a volume of 4% PFA, and processed for immunofluorescence.

The PC-I transport assay was performed in human fibroblasts as previously described (Venditti *et al*, 2012). For our purposes, cells were treated with SA (300  $\mu$ M) for 120 min at 40°C and analyzed 10 min after the temperature switch (40–32°C). Cells were then fixed and stained with appropriate antibodies.

### Electron microscopy

EM samples were prepared as previously described (D'Angelo *et al*, 2007). Briefly, cells were fixed by adding to the culture medium the same volume of a mixture of PHEM buffer (10 mM EGTA, 2 mM MgCl<sub>2</sub>, 60 mM PIPES, 25 mM HEPES, pH 6.9), 4% paraformaldehyde, 2% glutaraldehyde for 2 h, and then stored in storage solution (PHEM buffer, 0.5% paraformaldehyde) overnight. After washing with 0.15 M glycine buffer in PBS, the cells were scraped and pelleted by centrifugation, embedded in 10% gelatin, cooled on ice, and cut into 0.5-mm blocks. The blocks were infused with 2.3 M sucrose and trimmed with an ultramicrotome (Leica Ultracut R) at –120°C using a dry diamond knife.

### Quantitative real-time PCR

Real-time quantitative PCR (qRT-PCR) was carried out with the LightCycler 480 SYBR Green I mix (Roche) using the LightCycler 480 II detection system (Roche) with the following conditions: 95°C, 10 min; (95°C, 10 s; 60°C, 10 s; 72°C, 15 s)  $\times$  45 cycles. For expression studies, the qRT-PCR results were normalized against an internal control (HPRT1). Oligonucleotides used for qRT-PCR are listed in Appendix Table S2.

### Quantification and statistical analysis of data

Statistical details and sample numbers of IF and biochemical data are reported in figure legends. Quantification data were usually calculated from at least three biological replicates. Differences among groups were performed with one-way ANOVA; differences with respect to control were calculated by Dunnett's test or using the unpaired Student's *t*-test when applicable. Statistical analyses were performed with the GraphPad Prism software. All data are reported as mean  $\pm$  s.e.m. or  $\pm$  s.d. as indicated in the figure legends.

### Data availability

The mass spectrometry proteomics data have been deposited to the ProteomeXchange Consortium via the PRIDE [ID: 30395289] partner

repository with the dataset identifier PXD014395 (<http://www.ebi.ac.uk/pride/archive/projects/PXD014395>).

**Expanded View** for this article is available online.

## Acknowledgements

We thank Rossella Venditti for helpful discussion and for help in preparing the figures, Andrea Ballabio, Carmine Settembre, Leandro Raul Soria, Maria Chiara Masone, and Graciana Diez Roux for helpful discussion. We thank the TIGEM proteomics facility. MADM acknowledges the support of Telethon (grant TGM11CB1), the Italian Association for Cancer Research (AIRC, grant IG2013\_14761), European Research Council Advanced Investigator grant no. 670881 (SYSTEMET).

## Author contributions

FZ and MADM conceived the work. FZ planned and analyzed most of the experiments, CW performed experiments on yeast, GDT performed gel filtration, and Sec31-IP, MS provided technical support, PP and MM performed MS/MS analysis, DD helped with cell culture, SPV performed cell proliferation and flow cytometry assays, RDC and MF analyzed MS/MS data, AR helped in performing cell death assay, MAS provided podocytes cell line, EP performed EM analyses, LG designed the script for high-content analysis, and FZ and MADM conceptualized the work and strategy and wrote the manuscript.

## Conflict of interest

The authors declare that they have no conflict of interest.

## References

- Aguilera-Gomez A, Zacharogianni M, van Oorschot MM, Genau H, Grond R, Veenendaal T, Sinsimer KS, Gavis EA, Behrends C, Rabouille C (2017) Phospho-Rasputin stabilization by Sec16 is required for stress granule formation upon amino acid starvation. *Cell Rep* 20: 935–948
- Anderson P, Kedersha N (2002) Stressful initiations. *J Cell Sci* 115: 3227–3234
- Anderson P, Kedersha N (2008) Stress granules: the Tao of RNA triage. *Trends Biochem Sci* 33: 141–150
- Arimoto K, Fukuda H, Imajoh-Ohmi S, Saito H, Takekawa M (2008) Formation of stress granules inhibits apoptosis by suppressing stress-responsive MAPK pathways. *Nat Cell Biol* 10: 1324–1332
- Asghar U, Witkiewicz AK, Turner NC, Knudsen ES (2015) The history and future of targeting cyclin-dependent kinases in cancer therapy. *Nat Rev Drug Discov* 14: 130–146
- Aulas A, Fay MM, Szaflarski W, Kedersha N, Anderson P, Ivanov P (2017) Methods to classify cytoplasmic foci as mammalian stress granules. *J Vis Exp* e55656 <https://doi.org/10.3791/55656>
- Ballock RT, O'Keefe RJ (2003) The biology of the growth plate. *J Bone Joint Surg Am* 85: 715–726
- Bi X, Mancias JD, Goldberg J (2007) Insights into COPII coat nucleation from the structure of Sec23•Sar1 complexed with the active fragment of Sec31. *Dev Cell* 13: 635–645
- Catara G, Grimaldi G, Schembri L, Spano D, Turacchio G, Lo Monte M, Beccari AR, Valente C, Corda D (2017) PARP1-produced poly-ADP-ribose causes the PARP12 translocation to stress granules and impairment of Golgi complex functions. *Sci Rep* 7: 14035
- Chen D, Gibson ES, Kennedy MJ (2013) A light-triggered protein secretion system. *J Cell Biol* 201: 631–640
- Choi MY, Chan CC, Chan D, Luk DK, Cheah KD, Tanner JA (2009) Biochemical consequences of sedlin mutation that cause spondyloepiphyseal dysplasia tarda. *Biochem J* 423: 233–242
- D'Angelo G, Polishchuk E, Di Tullio G, Santoro M, Di Campli A, Godi A, West G, Bielawski J, Chuang CC, van der Spoel AC *et al* (2007) Glycosphingolipid synthesis requires FAPP2 transfer of glucosylceramide. *Nature* 449: 62–67
- D'Arcangelo JG, Stahmer KR, Miller EA (2013) Vesicle-mediated export from the ER: COPII coat function and regulation. *Biochim Biophys Acta* 1833: 2464–2472
- David A, Dolan BP, Hickman HD, Knowlton JJ, Clavarino G, Pierre P, Bennink JR, Yewdell JW (2012) Nuclear translation visualized by ribosome-bound nascent chain puromycylation. *J Cell Biol* 197: 45–57
- De Leo MG, Staiano L, Vicinanza M, Luciani A, Carissimo A, Mutarelli M, Di Campli A, Polishchuk E, Di Tullio G, Morra V *et al* (2016) Autophagosomal lysosome fusion triggers a lysosomal response mediated by TLR9 and controlled by OCRL. *Nat Cell Biol* 18: 839–850
- Dephoure N, Zhou C, Villén J, Beausoleil SA, Bakalarski CE, Elledge SJ, Gygi SP (2008) A quantitative atlas of mitotic phosphorylation. *Proc Natl Acad Sci USA* 105: 10762–10767
- Dubois T, Paléotti O, Mironov AA, Fraiser V, Stradal TEB, De Matteis MA, Franco M, Chavrier P (2005) Golgi-localized GAP for Cdc42 functions downstream of ARF1 to control Arp2/3 complex and F-actin dynamics. *Nat Cell Biol* 7: 353–364
- Farhan H, Wendeler MW, Mitrovic S, Fava E, Silberberg Y, Sharan R, Zerial M, Hauri H-P (2010) MAPK signaling to the early secretory pathway revealed by kinase/phosphatase functional screening. *J Cell Biol* 189: 997–1011
- Franzmann TM, Alberti S (2019) Protein phase separation as a stress survival strategy. *Cold Spring Harb Perspect Biol* 11: a034058
- Ge L, Zhang M, Kenny SJ, Liu D, Maeda M, Saito K, Mathur A, Xu K, Schekman R (2017) Remodeling of ER-exit sites initiates a membrane supply pathway for autophagosome biogenesis. *EMBO Rep* 18: 1586–1603
- Gedeon AK, Colley A, Jamieson R, Thompson EM, Rogers J, Sillence D, Tiller GE, Mulley JC, Géczy J (1999) Identification of the gene (SEDL) causing X-linked spondyloepiphyseal dysplasia tarda. *Nat Genet* 22: 400–404
- Gorur A, Yuan L, Kenny SJ, Baba S, Xu K, Schekman R (2017) COPII-coated membranes function as transport carriers of intracellular procollagen I. *J Cell Biol* 216: 1745–1759
- Harripaul R, Vasli N, Mikhailov A, Rafiq MA, Mittal K, Windpassinger C, Sheikh TI, Noor A, Mahmood H, Downey S *et al* (2018) Mapping autosomal recessive intellectual disability: combined microarray and exome sequencing identifies 26 novel candidate genes in 192 consanguineous families. *Mol Psychiatry* 23: 973–984
- Henrotin YE, Bruckner P, Pujol JP (2003) The role of reactive oxygen species in homeostasis and degradation of cartilage. *Osteoarthritis Cartilage* 11: 747–755
- Holt LJ, Tuch BB, Villén J, Johnson AD, Gygi SP, Morgan DO (2009) Global analysis of Cdk1 substrate phosphorylation sites provides insights into evolution. *Science* 325: 1682–1686
- Hu H, Gourguechon S, Wang CC, Li Z (2016) The G1 cyclin-dependent kinase CRK1 in *Trypanosoma brucei* regulates anterograde protein transport by phosphorylating the COPII subunit Sec31. *J Biol Chem* 291: 15527–15539
- Imai K, Hao F, Fujita N, Tsuji Y, Oe Y, Araki Y, Hamasaki M, Noda T, Yoshimori T (2016) Atg9A trafficking through the recycling endosomes is required for autophagosome formation. *J Cell Sci* 129: 3781–3791

- Jain S, Wheeler JR, Walters RW, Agrawal A, Barsic A, Parker R (2016) ATPase modulated stress granules contain a diverse proteome and substructure. *Cell* 164: 487–498
- Kapetanovich L, Baughman C, Lee TH (2005) Nm23H2 facilitates coat protein complex II assembly and endoplasmic reticulum export in mammalian cells. *Mol Biol Cell* 16: 835–848
- Khattak NA, Mir A (2014) Computational analysis of TRAPPC9: candidate gene for autosomal recessive non-syndromic mental retardation. *CNS Neurol Disord Drug Targets* 13: 699–711
- Kim JJ, Lipatova Z, Segev N (2016) TRAPP Complexes in secretion and autophagy. *Front Cell Dev Biol* 4: 20
- Koehler K, Milev MP, Prematilake K, Reschke F, Kutzner S, Jühlen R, Landgraf D, Utine E, Hazan F, Diniz G et al (2017) A novel TRAPPC11 mutation in two Turkish families associated with cerebral atrophy, global retardation, scoliosis, achalasia and alacrima. *J Med Genet* 54: 176–185
- Lamb CA, Nühlen S, Judith D, Frith D, Snijders AP, Behrends C, Tooze SA (2016) TBC1D14 regulates autophagy via the TRAPP complex and ATG9 traffic. *EMBO J* 35: 281–301
- van Leeuwen W, van der Krift F, Rabouille C (2018) Modulation of the secretory pathway by amino-acid starvation. *J Cell Biol* 217: 2261–2271
- Li C, Luo X, Zhao S, Siu GK, Liang Y, Chan HC, Satoh A, Yu SS (2017) COPI-TRAPP II activates Rab18 and regulates its lipid droplet association. *EMBO J* 36: 441–457
- Lord C, Bhandari D, Menon S, Ghassemian M, Nycz D, Hay J, Ghosh P, Ferro-Novick S (2011) Sequential interactions with Sec23 control the direction of vesicle traffic. *Nature* 473: 181–186
- Mahfouz H, Ragnini-Wilson A, Venditti R, De Matteis MA, Wilson C (2012) Mutational analysis of the yeast TRAPP subunit Trs20p identifies roles in endocytic recycling and sporulation. *PLoS One* 79: e41408
- Malumbres M (2014) Cyclin-dependent kinases. *Genome Biol* 15: 122
- Markmiller S, Soltanieh S, Server KL, Mak R, Jin W, Fang MY, Luo EC, Krach F, Yang D, Sen A et al (2018) Context-dependent and disease-specific diversity in protein interactions within stress granules. *Cell* 172: 590–604
- Michalski A, Damoc E, Hauschild JP, Lange O, Wieghaus A, Makarov A, Nagaraj N, Cox J, Mann M, Horning S (2011) Mass spectrometry-based proteomics using Q Exactive, a high-performance benchtop quadrupole Orbitrap mass spectrometer. *Mol Cell Proteomics* 10: M111.011015
- Milev MP, Grout ME, Saint-Dic D, Cheng Y-HH, Glass IA, Hale CJ, Hanna DS, Dorschner MO, Prematilake K, Shaag A et al (2017) Mutations in TRAPPC12 manifest in progressive childhood encephalopathy and Golgi dysfunction. *Am J Hum Genet* 101: 291–299
- Milev MP, Graziano C, Karall D, Kuper WFE, Al-Deri N, Cordelli DM, Haack TB, Danhauser K, Luso A, Palombo F et al (2018) Bi-allelic mutations in TRAPPC2L result in a neurodevelopmental disorder and have an impact on RAB11 in fibroblasts. *J Med Genet* 55: 753–764
- Mironov AA, Beznoussenko GV, Nicoziani P, Martella O, Trucco A, Kweon H-S, Giandomenico DD, Polishchuk RS, Fusella A, Lupetti P et al (2001) Small cargo proteins and large aggregates can traverse the Golgi by a common mechanism without leaving the lumen of cisternae. *J Cell Biol* 155: 1225–1238
- Mohamoud HS, Ahmed S, Jelani M, Alrayes N, Childs K, Vadgama N, Almrhamhi MM, Al-Aama JY, Goodbourn S, Nasir J (2018) A missense mutation in TRAPPC6A leads to build-up of the protein, in patients with a neurodevelopmental syndrome and dysmorphic features. *Sci Rep* 8: 2053
- Moujalled D, James JL, Yang S, Zhang K, Duncan C, Moujalled DM, Parker SJ, Caragounis A, Lidgerwood G, Turner BJ et al (2015) Phosphorylation of hnRNP K by cyclin-dependent kinase 2 controls cytosolic accumulation of TDP-43. *Hum Mol Genet* 24: 1655–1669
- Olsen JV, Blagoev B, Gnäd F, Macek B, Kumar C, Mortensen P, Mann M (2006) Global, *in vivo*, and site-specific phosphorylation dynamics in signaling networks. *Cell* 127: 635–648
- Palmer KJ, Konkel JE, Stephens DJ (2005) PCTAIRE protein kinases interact directly with the COPII complex and modulate secretory cargo transport. *J Cell Sci* 118: 3839–3847
- Protter DSW, Parker R (2016) Principles and properties of stress granules. *Trends Cell Biol* 26: 668–679
- Rabouw HH, Langereis MA, Anand AA, Visser LJ, de Groot RJ, Walter P, van Kuppeveld FJM (2019) Small molecule ISRIB suppresses the integrated stress response within a defined window of activation. *Proc Natl Acad Sci USA* 116: 2097–2102
- Ramírez-Peinado S, Ignashkova TI, van Raam BJ, Baumann J, Sennott EL, Gendarme M, Lindemann RK, Starnbach MN, Reiling JH (2017) TRAPPC13 modulates autophagy and the response to Golgi stress. *J Cell Sci* 130: 2251–2265
- Rappsilber J, Ishihama Y, Mann M (2003) Stop and go extraction tips for matrix-assisted laser desorption/ionization, nanoelectrospray, and LC/MS sample pretreatment in proteomics. *Anal Chem* 75: 663–670
- Riback JA, Katanski CD, Kear-Scott JL, Pilipenko EV, Rojek AE, Sosnick TR, Drummond DA (2017) Stress-triggered phase separation is an adaptive, evolutionarily tuned response. *Cell* 168: 1028–1040
- Sacher M, Shahrzad N, Kamel H, Milev MP (2018) TRAPPopathies: an emerging set of disorders linked to variations in the genes encoding transport protein particle (TRAPP)-associated proteins. *Traffic* 20: 5–26
- Saleem MA, O'Hare MJ, Reiser J, Coward RJ, Inward CD, Farren T, Xing CY, Ni L, Mathieson PW, Mundel P (2002) A conditionally immortalized human podocyte cell line demonstrating nephrin and podocin expression. *J Am Soc Nephrol* 13: 630–638
- Saurus P, Kuusela S, Dumont V, Lehtonen E, Fogarty CL, Lassenius MI, Forsblom C, Lehto M, Saleem MA, Groop P-H et al (2016) Cyclin-dependent kinase 2 protects podocytes from apoptosis. *Sci Rep* 6: 21664
- Scrivens PJ, Noueihed B, Shahrzad N, Hul S, Brunet S, Sacher M (2011) C4orf41 and TTC-15 are mammalian TRAPP components with a role at an early stage in ER-to-Golgi trafficking. *Mol Biol Cell* 22: 2083–2093
- Shevchenko A, Tomas H, Havlis J, Olsen JV, Mann M (2006) In-gel digestion for mass spectrometric characterization of proteins and proteomes. *Nat Protoc* 1: 2856–2860
- Sidrauski C, McGeachy AM, Ingolia NT, Walter P (2015) The small molecule ISRIB reverses the effects of eIF2 $\alpha$  phosphorylation on translation and stress granule assembly. *eLife* 4: e05033
- Takahashi M, Higuchi M, Matsuki H, Yoshita M, Ohsawa T, Oie M, Fujii M (2013) Stress granules inhibit apoptosis by reducing reactive oxygen species production. *Mol Cell Biol* 33: 815–829
- Thedieck K, Holzwarth B, Prentzell MT, Boehlke C, Kläsener K, Ruf S, Sonntag AG, Maerz L, Grellscheid S-N, Kremmer E et al (2013) Inhibition of mTORC1 by astrin and stress granules prevents apoptosis in cancer cells. *Cell* 154: 859–874
- Tiller GE, Hannig VL, Dozier D, Carrel L, Trevarthen KC, Wilcox WR, Mundlos S, Haines JL, Gedeon AK, Gecz J (2001) A recurrent RNA-splicing mutation in the SEDL gene causes X-linked spondyloepiphyseal dysplasia tarda. *Am J Hum Genet* 68: 1398–1407
- Tillmann KD, Reiterer V, Baschieri F, Hoffmann J, Millarte V, Hauser MA, Mazza A, Atias N, Legler DF, Sharan R et al (2015) Regulation of Sec16 levels and dynamics links proliferation and secretion. *J Cell Sci* 128: 670–682

- Tisdale EJ, Bourne JR, Khosravi-Far R, Der CJ, Balch WE (1992) GTP-binding mutants of rab1 and rab2 are potent inhibitors of vesicular transport from the endoplasmic reticulum to the Golgi complex. *J Cell Biol* 119: 749–761
- Venditti R, Scanu T, Santoro M, Di Tullio G, Spaar A, Gaibisso R, Beznoussenko GV, Mironov AA, Mironov A, Zelante L et al (2012) Sedlin controls the ER export of procollagen by regulating the Sar1 cycle. *Science* 337: 1668–1672
- Vicinanza M, Di Campli A, Polishchuk E, Santoro M, Di Tullio G, Godi A, Levtschenko E, De Leo MG, Polishchuk R, Sandoval L et al (2011) OCRL controls trafficking through early endosomes via PtdIns4,5P<sub>2</sub>-dependent regulation of endosomal actin. *EMBO J* 30: 4970–4985
- Westlake CJ, Baye LM, Nachury MV, Wright KJ, Ervin KE, Phu L, Chalouni C, Beck JS, Kirkpatrick DS, Slusarski DC et al (2011) Primary cilia membrane assembly is initiated by Rab11 and transport protein particle II (TRAPP II) complex-dependent trafficking of Rabin8 to the centrosome. *Proc Natl Acad Sci USA* 108: 2759–2764
- Wheeler JR, Matheny T, Jain S, Abrisch R, Parker R (2016) Distinct stages in stress granule assembly and disassembly. *eLife* 5: e18413
- Wilson BS, Nuoffer C, Meinkoth JL, McCaffery M, Feramisco JR, Balch WE, Farquhar MG (1994) A Rab1 mutant affecting guanine nucleotide exchange promotes disassembly of the Golgi apparatus. *J Cell Biol* 125: 557–571
- Wippich F, Bodenmiller B, Trajkovska MG, Wanka S, Abersold R, Pelkmans L (2013) Dual specificity kinase DYRK3 couples stress granule condensation/dissolution to mTORC1 signaling. *Cell* 152: 791–805
- Yamasaki A, Menon S, Yu S, Barrowman J, Meerloo T, Oorschot V, Klumperman J, Satoh A, Ferro-Novick S (2009) mTrs130 is a component of a mammalian TRAPP II complex, a Rab1 GEF that binds to COPI-coated vesicles. *Mol Biol Cell* 20: 4205–4215
- Youn JY, Dunham WH, Hong SJ, Knight JD, Bashkurov M, Chen GI, Bagci H, Rathod B, MacLeod G, Eng SW et al (2018) High-density proximity mapping reveals the subcellular organization of mRNA-associated granules and bodies. *Mol Cell* 69: 517–532
- Yu S, Satoh A, Pypaert M, Mullen K, Hay JC, Ferro-Novick S (2006) mBet3p is required for homotypic COPII vesicle tethering in mammalian cells. *J Cell Biol* 174: 359–368
- Zacharogianni M, Aguilera-Gomez A, Veenendaal T, Smout J, Rabouille C (2014) A stress assembly that confers cell viability by preserving ERES components during amino-acid starvation. *eLife* 3: e04132
- Zou S, Liu Y, Zhang XQ, Chen Y, Ye M, Zhu X, Yang S, Lipatova Z, Liang Y, Segev N (2012) Modular TRAPP complexes regulate intracellular protein trafficking through multiple Ypt/Rab GTPases in *Saccharomyces cerevisiae*. *Genetics* 191: 451–460
- Zuscik MJ, Hilton MJ, Zhang X, Chen D, O'Keefe RJ (2008) Regulation of chondrogenesis and chondrocyte differentiation by stress. *J Clin Invest* 118: 429–438



**License:** This is an open access article under the terms of the Creative Commons Attribution 4.0 License, which permits use, distribution and reproduction in any medium, provided the original work is properly cited.